Chapter 8
Relationship Between Structure and Mechanics for Membranous Tissues

Jessica W.Y. Jor, Thiranja P. Babarenda Gamage, Poul M.F. Nielsen, Martyn P. Nash, and Peter J. Hunter

Abstract Professor Yoram Lanir has pioneered the development of structurally based constitutive relations to describe the stress–strain response of soft biological tissues. This approach relates the mechanical response of the tissue to the intrinsic micro-structural properties of its constituents, such as collagen. This article summarises some of the work by the Auckland Bioengineering Institute contributing towards the goal of understanding the structure–function relationship of soft membranous tissue. Key aspects of our work are to (1) develop constitutive relations based on quantitative information of tissue structure; and (2) use rich sets of experimental data to aid in accurate and reliable constitutive parameter identification. We first outline several common techniques to quantify tissue structure, such as collagen fibre orientations. A detailed description of an extended-volume imaging system, developed in our laboratory, is then provided along with a few application examples. The gathered imaging data is incorporated into structural constitutive models by means of fitting to mathematical distributions. Based upon the observations made from some imaging studies, a conceptual fibre distribution model is proposed for modelling the collagen network in skin. We then introduce a selection of constitutive models, which have been developed to characterise the mechanical behaviour of soft connective tissues (skin in particular), with particular emphasis on structurally based models. Finite element models, used with appropriate constitutive relations, provide a means of interpreting experimental results. Some of our recent efforts in developing instrumentation to measure the two-dimensional and three-dimensional response of soft tissues are described. This includes a biaxial tensile rig, which is capable of deforming membranes in up to 16 directions, and a force-sensitive micro-robot. We highlight some of the challenges often associated with constitutive parameter identification using commonly used

J.W.Y. Jor (✉) • T.P.B. Gamage • P.J. Hunter
Auckland Bioengineering Institute, The University of Auckland, Auckland, New Zealand
e-mail: j.jor@auckland.ac.nz; psam012@aucklanduni.ac.nz; p.hunter@auckland.ac.nz

P.M.F. Nielsen • M.P. Nash
Auckland Bioengineering Institute and Department of Engineering Science,
The University of Auckland, Auckland, New Zealand
e-mail: p.nielsen@auckland.ac.nz; martyn.nash@auckland.ac.nz

G.S. Kassab, M.S. Sacks (eds.), *Structure-Based Mechanics of Tissues and Organs*,
DOI 10.1007/978-1-4899-7630-7_8

model based fitting approaches. These issues were examined and illustrated in depth by performing controlled studies on silicon gel phantoms, which allowed us to focus our attention solely on the identification problem. Lastly, future directions of applying structurally based models to understanding the biomechanics of soft tissues are discussed.

8.1 Introduction

More than three decades ago, Professor Yoram Lanir proposed the use of structural constitutive relations to describe the stress–strain response of soft connective tissues, thereby highlighting the important relationship between tissue composition and behaviour. In essence, structural models aim to take into consideration the intrinsic micro-structural properties of fibres (including fibre undulation and orientation) when deriving constitutive equations. In the skin, networks of collagen (60–80 % of dry weight) and elastin (1–4 % of dry weight) fibres are embedded in a fluid-like ground substance (70–90 % of skin volume), comprised of water and proteoglycan molecules (Wilkes et al. 1973; Silver et al. 1992). Collagen fibres are non-uniformly undulated in their natural state and form a three-dimensional interwoven network throughout the depth of the dermis (Finlay 1969). Elastin fibres are straight in their natural state and are less stiff compared with collagen fibres. They are capable of reversibly withstanding stretches to more than 100 % and hence provide the skin with its ability to recoil to its original shape after being stretched (Carton et al. 1962). Experiments in which elastin and ground substance were digested suggested that elastin's contribution to the mechanical response of skin is only significant at low strains, while the overall contribution from the ground substance is small (Daly 1969; Harkness and Harkness 1959). It is widely accepted that collagen is the predominant stress-bearing component in skin at high strains (Brown 1973). It has been observed in tendons that undulated collagen fibres became gradually recruited upon stretch, giving rise to the tissue nonlinearity commonly observed during the toe region of the stress–strain curve (Abrahams 1967). This is due to an increasing number of fibres being gradually straightened, and then stretched, contributing to the overall macroscopic tissue stiffness. In addition, tissue anisotropy is predominantly a result of the non-uniform orientation of the fibres.

Because there is a close relationship between tissue structure and mechanical behaviour, structural constitutive relations are advantageous by providing a means to directly relate model parameters to the underlying tissue microstructure. Prior to the use of structural models, the most common approach to modelling the elastic response of soft biological tissue was to use phenomenological models. In phenomenological models, mathematical expressions are chosen to best fit experimental data or reflect material behaviour, such as the widely used power

(Kenedi et al. 1965) and exponential forms (Tong and Fung 1976). A major disadvantage is that the parameters obtained for phenomenological models cannot be directly related to specific biological constituents.

Although the skin is used as a representative tissue throughout this paper to demonstrate the fundamental concepts of structural models, the observed structure–function relationship is applicable across other soft connective tissues. To date, structural approaches to modelling soft tissues have been employed to investigate the mechanical properties of various organs and tissues, including skin (Lanir 1983; Lokshin and Lanir 2009a,b; Jor et al. 2011a), tendon (Hurschler et al. 1997), pericardium (Sacks 2003), arterial walls (Holzapfel et al. 2002), passive myocardium (Horowitz et al. 1988; Holzapfel and Ogden 2009), and heart valves (Billiar and Sacks 2000; Freed et al. 2005; Gasser et al. 2006). This paper summarises some of our published works on characterising the structural and mechanical properties of soft tissues by bringing together imaging, experimental and computational modelling techniques into a single framework.

In Sect. 8.2, we first outline several common techniques to quantify tissue structure, such as collagen fibre orientations. A detailed description of an extended-volume imaging system, developed in our laboratory, is then provided along with a few application examples. The gathered imaging data is incorporated into structural constitutive models by means of fitting to mathematical distributions. Based upon the observations made from some imaging studies, a conceptual fibre distribution model is proposed for modelling the collagen network in skin. We then introduce, in Sect. 8.3, a selection of constitutive models, which have been developed to characterise the mechanical behaviour of soft connective tissues (skin in particular), with particular emphasis on structurally based models. Finite element (FE) models, used with appropriate constitutive relations, provide a means of interpreting experimental results. In Sect. 8.4, we describe some of our recent efforts in developing instrumentation to measure the two-dimensional (2D) and three-dimensional (3D) response of soft tissues. This includes a biaxial tensile rig, which is capable of deforming membranes in up to 16 directions, and a force-sensitive micro-robot. Several experimental studies on skin tissues will be summarised in this section. In Sect. 8.5, we highlight some of the challenges often associated with constitutive parameter identification using model based fitting approaches. These issues were examined and illustrated in depth by performing controlled studies on silicon gel phantoms, which allowed us to focus our attention solely on the identification problem. Finally, Sect. 8.6 is devoted to discussing future directions of applying structurally based models to soft tissues.

8.2 Quantification of Tissue Structure

One of the major challenges in modelling soft connective tissues is the difficulty in reliable and meaningful determination of constitutive parameters. To address this issue, quantification of structural parameters is therefore useful in minimising

the effects of structural variability in constitutive modelling. Recognising the importance of tissue microstructure and its relationship to the mechanical behaviour has led to an increasing number of studies looking to quantify the structural properties of soft connective tissues. The structure of collagen networks has been studied extensively in both human and animal issues (Craik and McNeil 1964; Marcarian and Calhoun 1966; Finlay 1969; Meyer et al. 1982). Of particular interest is the orientation of collage fibres, due to its important role in providing the mechanical stability of the tissue and its contribution to the overall tissue behaviour.

Collagen fibres are rendered visible by traditional histological stains, such as Hematoxylin-Eosin, Pontamine Sky Blue-Eosin, Elastica van Gieson and picrosirius red (PSR). Microscopic techniques have been developed to visualise collagen fibres, such as polarised light microscopy (Junquiera et al. 1982), fluorescence microscopy (Dolber and Spach 1993; MacKenna et al. 1996) and confocal laser scanning microscopy (CLSM) (Young et al. 1998). However, these conventional microscopic techniques are often limited to relatively small regions in the tissue, making it difficult to quantify fibre structure on a larger scale. Early microscopic studies have suggested that collagen fibres are arranged in an organised, interwoven structure in the skin. In order to quantify fibre orientations, several studies represent the degree of fibre anisotropy using a relative measure, often referred to as the "collagen alignment index". The techniques used to quantify the degree of collagen anisotropy included fitting ovals to binary images of skin samples viewed under polarised light and taking the major axes of fitted ovals as the alignment index parameter (Melis et al. 2002), performing Fourier analysis on cross-sectional images of skin samples, and estimating the alignment index as the width-height ratio of the power spectrum (van Zuijlen et al. 2003; Noorlander et al. 2002). Typically, an alignment index value of zero indicates an isotropic distribution of fibres while a value of one indicates perfectly aligned fibres. Despite being able to describe the extent of fibre orientation anisotropy in a quantitative manner, the above studies do not provide fibre orientations with respect to the tissue material axes (i.e. an absolute orientation measure). Therefore, such data cannot be used for fitting to statistical distribution functions to model fibre orientation.

Sacks et al. (1997) characterised collagen orientations in samples of pericardium and intestinal submucosa using a small angle light scattering (SALS) device. In brief, a Helium–Neon (HeNe) laser was passed through the thin connective tissues. HeNe was chosen because its wavelength ($\lambda = 632.8\,\text{nm}$) is within an order of magnitude of the diameter of the collagen and elastin fibres. As the laser is passed through the tissue, a pattern is formed as a result of light being scattered by the fibrous structures. The angular distribution of collagen fibres $R(\theta)$ can then be directly correlated to the angular distribution of scattered light $I(\theta)$. The experimentally derived angular distribution of collagen fibres was directly incorporated into structural constitutive models to predict the biaxial mechanical response of bovine pericardium. Although the SALS technique is suitable for determining collagen fibre orientations in thin connective tissues, such as the pericardium and heart valves, it is not appropriate for skin tissues. Meijer (1997) found that the charge-coupled device (CCD) camera employed in the SALS technique was not sensitive

enough to detect scattered light from stained collagen fibres in rat skin tissues, which were approximately 380 μm thick. Due to its projective nature, the SALS technique is also limited to the detection of collagen orientations in the in-plane direction only, i.e. it cannot provide structural information in the transverse direction nor can it be used to build a 3D dataset of images.

The development of structurally based computational models of biological tissue relies on the ability to quantify and visualise 3D tissue structure across a large range of resolutions and scales. For imaging of large tissue volumes, it is often challenging to address the problems associated with image registration, section distortion, and realignment. To this end, the motivation to acquire high resolution images in a high throughput manner has led to the development of a novel automated CLSM imaging system by our group (Sands et al. 2005).

8.2.1 Extended-Volume CLSM

The automated extended-volume imaging system consists of a high precision XYZ translation stage, to which the specimen is mounted and imaged using a modified CLSM (Leica Microsystems AG, Germany) (Fig. 8.1). The use of the translation stage enables the acquisition of images over larger regions than previously possible using conventional microscope systems. It avoids the need to remove the specimen from the microscope stage for manual sectioning, thus re-positioning and alignment of the specimen is not required at each step. The dimensions that can be imaged in the Z direction using conventional CLSM is often limited by absorption and scattering of light in the specimen. To overcome this limitation, extended imaging into the depth of the tissue is enabled by removing the upper surface of the specimen using a specialised ultramill (Leica Microsystems). The translation stage, image acquisition and tissue removal are controlled simultaneously by specialised hardware and software to enable automated acquisition of a grid of image stacks to form a 3D image dataset.

The CLSM system has been used to visualise the collagen fibre structure in various soft tissues, including myocardial tissue (Sands et al. 2005; Pope et al. 2008), rat cortex tissues (Sands et al. 2005), engineered heart valves tissues (Eckert et al. 2011) and cardiac trabeculae carneae (Sands et al. 2011). To give a representative example of the capabilities of the CLSM system, the image acquisition of ventricular tissue will be presented. Rat hearts were excised, mounted on a Langedorff apparatus, and perfused with oxygenated Tyrode's solution. In a relaxed state, the heart was arrested and perfused with Bouin's fixative solution. To render collagen fibres visible, the heart was then perfused with collagen-specific stain PSR (Sweat et al. 1964). A transmural 3 mm section from the LV free wall was cut and embedded in Agar 100 resin for imaging. A 16x/0.5 NA Plan Fluotar oil-immersion lens was used to obtain 512 pixel × 512 pixel slices with lateral resolution of 1.22 μm. To image PSR-stained samples, a rhodamine filter set (excitation wavelength at 568 nm; high pass detection filter at 590 nm) was used, with 8× averaging for the ventricular

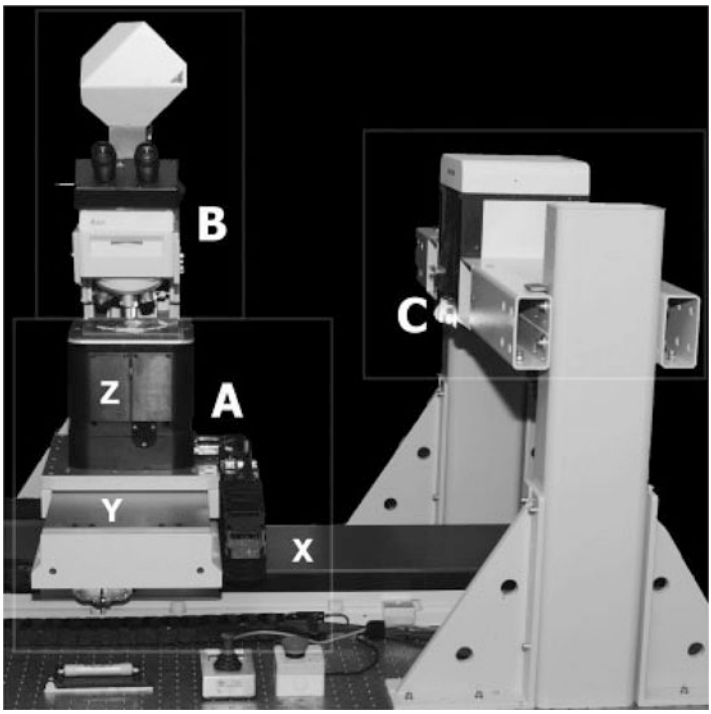

Fig. 8.1 The extended-volume confocal microscope imaging system consists of a high-precision three-axis translation stage (labelled as **A** with individual **X**,**Y** and **Z** translation stages), confocal microscope unit (**B**), and the ultramill (**C**). Reproduced with permission from Sands et al. (2005)

samples. A region of interest (5 × 3 mm) was specified to form a regular X-Y grid of overlapping slices. The depth to which the specimen may be imaged before the upper surface is milled was determined to be 35 μm, allowing 28 planes to be acquired at 1.22 μm spacing in the Z direction. At each milling step, 30 μm of tissue was removed. The volume rendering of the 3D reconstruction of the imaged specimen, covering 4.25 × 1.12 × 0.88 mm, is shown in Fig. 8.2. Brightly stained collagen fibres were shown to vary significantly in the transmural direction, and are densely arranged in sheets lining the epicardial and endocardial surfaces.

The imaging system has also been used to visualise collagen fibres in skin specimens (Jor et al. 2011b). Unlike cardiac tissues, stain penetration for the skin samples was achieved primarily via tissue diffusion (not via perfusion). However, because of the dense structure of the dermal tissue, stain penetration by means of diffusion was found to be limited in the direction of tissue depth. To overcome this problem, 30–60 μm thick transverse cryosections were obtained from the abdominal region of young pigs at four orientations (0°, 30°, 60°, 90°) with respect to the torso mid-line. Since the sample thickness was relatively thin, the milling procedure was omitted in this study. Skin sections were fixed in Bouin's solution, prior to staining in PSR. Images were acquired using the protocols described for myocardium tissues,

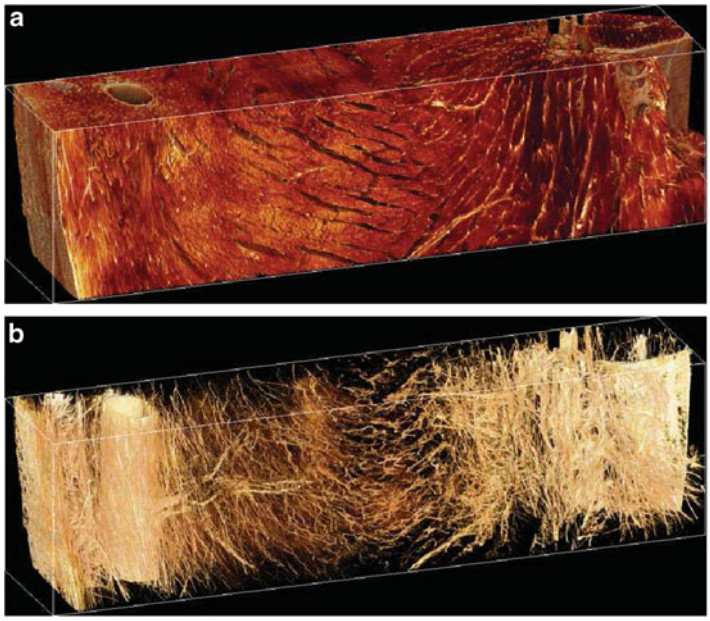

Fig. 8.2 (**a**) The volume rendering reconstruction of a transmural stack of myocardial tissue, and (**b**) with the collagen network revealed by adjusting for image transparency based upon intensity values. Reproduced with permission from Sands et al. (2005)

but using a 20× water immersion lens with 4× line averaging. The lateral resolution for the acquired images was 0.98 μm per pixel. Overlapping 512 pixel × 512 pixel images were acquired and montaged together to form a 3 × 2 mm slice mosaic at each z-depth. The imaging process was repeated at 1 μm steps throughout the entire tissue thickness, forming a stack of slice mosaics. For each tissue section, a maximum intensity projection was obtained from all slice mosaics through the entire z-depth.

Figure 8.3 shows a typical image of a PSR-stained sagittal section of porcine skin. CLSM images of pig skin in this study showed in the reticular dermis region thick collagen bundles crossing obliquely in two main directions, between epidermis and hypodermis. Smaller diameter fibres are interwoven between the main network. The oblique arrangement of collagen fibres is thought to be responsible for resisting in-plane shear deformation while allowing changes in thickness of the dermis as the skin is stretched or compressed. In contrast, thinner collagen bundles were found in a more parallel arrangement in the relatively thin papillary dermis layer as seen in Fig. 8.4. The collagen fibres were observed to form a dense and compact 3D meshwork in the dermis region. Such observations are consistent with early qualitative studies performed on pig skin using light microscopy and SEM (Mowafy and Cassens 1975; Meyer et al. 1982).

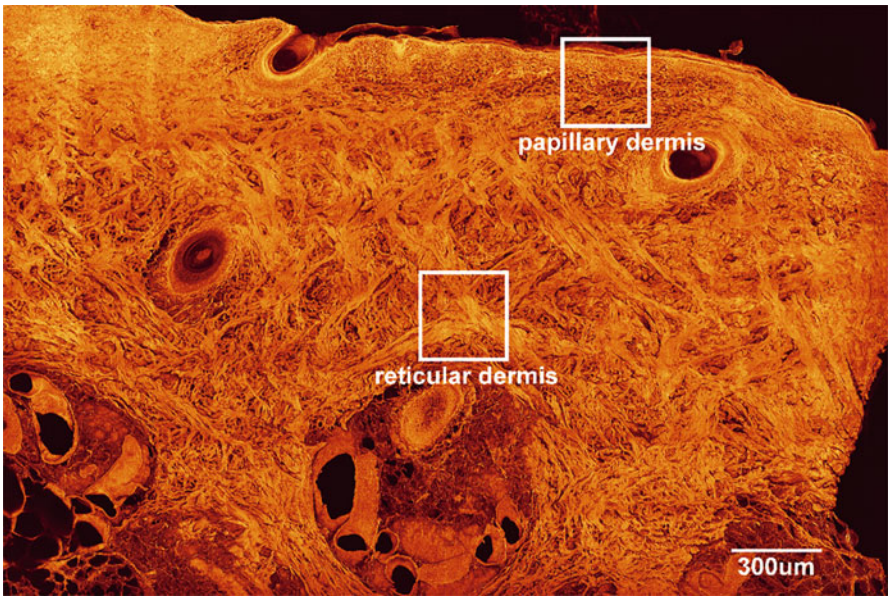

Fig. 8.3 Maximum intensity projection of a 60 μm sagittal section of picrosirius stained porcine skin, revealing the cross lattice arrangement of collagen fibres. Reproduced with permission from Jor et al. (2011b)

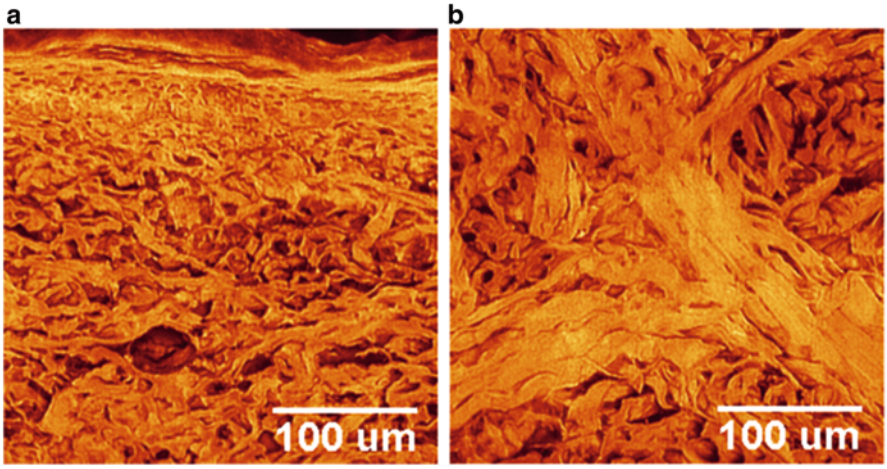

Fig. 8.4 300 × 300 μm cropped sections from Fig. 8.3: (**a**) thinner collagen fibre bundles are seen in the upper papillary dermis region; (**b**) much thicker collagen fibre bundles, arranged in a lattice structure, are found in the lower reticular dermis region. Reproduced with permission from Jor et al. (2011b)

8.2.2 Structure Tensor Approach

To analyse the structure of collagen of the acquired images of skin specimens, a structure-tensor approach was used to determine fibre orientations (Jahne 2004). The components of a structure tensor are the weighted sum of the first-order spatial derivatives of the image. The information within a local neighbourhood about the central point $\mathbf{x}$ is weighted by the window function $w(\mathbf{x}-\mathbf{x}')$

$$J_{pq}(\mathbf{x}) = \int_{-\infty}^{\infty} w(\mathbf{x}-\mathbf{x}') \left(\frac{\partial g(\mathbf{x}')}{\partial x_p} \frac{\partial g(\mathbf{x}')}{\partial x_q} \right) d\mathbf{x}' \tag{8.1}$$

where $g(\mathbf{x})$ represents the grey values and $\partial g(\mathbf{x}')/\partial x_p$ is the partial derivation along the p-axis direction.

The components of the structure tensor can be computed efficiently as a combination of linear convolution and nonlinear point operations. This involves convolving the image independently with partial derivative operators (D_p, D_q) associated with each coordinate (p, q), multiplying both images on a pixel basis prior to applying a smoothing operator (B) to the resultant image.

$$J_{pq} = B(D_p \times D_q) \tag{8.2}$$

After computing the structure tensor, an eigenvalue analysis is performed to extract local orientation vectors. For a 2D image, the form of the structure tensor is

$$\mathbf{J} = \begin{bmatrix} J_{xx} & J_{xy} \\ J_{xy} & J_{yy} \end{bmatrix} \tag{8.3}$$

The eigenvalue analysis involves only a single rotation from the image coordinate system to the principal axes coordinate system [Eq. (8.4)]. As a result, the two axes are aligned with the directions of the eigenvectors of the maximum and minimum eigenvalues, respectively.

$$\begin{bmatrix} J_x & 0 \\ 0 & J_y \end{bmatrix} = \begin{bmatrix} \cos\phi & -\sin\phi \\ \sin\phi & \cos\phi \end{bmatrix} \begin{bmatrix} J_{xx} & J_{xy} \\ J_{xy} & J_{yy} \end{bmatrix} \begin{bmatrix} \cos\phi & \sin\phi \\ -\sin\phi & \cos\phi \end{bmatrix} \tag{8.4}$$

By substitution of trigonometric identities, the orientation vector O in vectorial form can be written as

$$O = \begin{bmatrix} J_{yy} - J_{xx} \\ 2J_{xy} \end{bmatrix} \tag{8.5}$$

where the orientation angle is given by the phase of this vector (ϕ). As shown in Eq. (8.5), the components of the orientation vector are readily obtained from the components of the structure tensor and involve only one subtraction and one multiplication.

Fibre orientations in sagittal sections of porcine skin were defined with respect to the direction normal to the epidermis (ranging from $-\frac{\pi}{2}$ to $+\frac{\pi}{2}$), with clockwise angles from the Y-axis to X-axis in the imaging plane defined as positive. The structure-tensor algorithm was used to determine fibre orientations of a regular grid of 16 pixel $\times$ 16 pixel for each image projection, as shown in Fig. 8.5a. Areas containing non-collagenous features such as blood vessels, hair follicles and fat tissue were masked and excluded from the statistical analysis as shown in Fig. 8.5b.

8.2.3 Fitting Fibre Orientations

In order to incorporate micro-structural information into computational models, mathematical density distributions are employed in structural constitutive equations to represent the distributions of fibre undulation and orientations. One of the most common mathematical distributions used to represent circular data is the von Mises (VM) distribution, VM(μ, κ). The probability density distribution function of VM(μ, κ) is given by

$$R(\theta) = \frac{e^{\kappa \cos(\theta - \mu)}}{2\pi I_0(\kappa)} \quad 0 \leq \theta < 2\pi \quad 0 \leq \kappa < \infty \tag{8.6}$$

where

$$I_0(\kappa) = \frac{1}{2\pi} \int_0^{2\pi} \exp^{\kappa \cos(\phi - \mu)} d\phi \tag{8.7}$$

is the modified Bessel function of order zero. The parameter μ is the circular mean and κ is a measure of spread that is related to the inverse of the standard deviation in the conventional Gaussian distribution. As κ tends to zero, the distribution tends to a uniform distribution. As κ tends to large values, the distribution becomes concentrated about the mean orientation, μ.

Due to the bimodal nature of fibre orientations from porcine skin, a mixture of two symmetrical VM distributions was selected for fitting the acquired imaging data. The method of moments was used in this study to estimate parameters of the distribution (Spurr and Koutbeiy 1991). Figure 8.5c shows a representative histogram and fitted VM distributions to fibre data obtained from skin specimens aligned parallel to the torso mid-line. It was demonstrated that the two parameters of the distribution, the orientation mean and spread, may be directly determined using CLSM image analysis. An important advantage of this approach is that model parameters can be estimated directly from observable micro-structural features.

One important feature observed in the images was the presence of a distinct lattice pattern in the transverse samples. Based on fibre data obtained from a single sectioning orientation, there was insufficient information to deduce the collagen structure arrangement; thus, images from other sectioning orientations were required. Analysis of transverse sections excised at $0°, 30°, 60°$ and $90°$ relative to the torso mid-line revealed that the distributions of fibre orientations

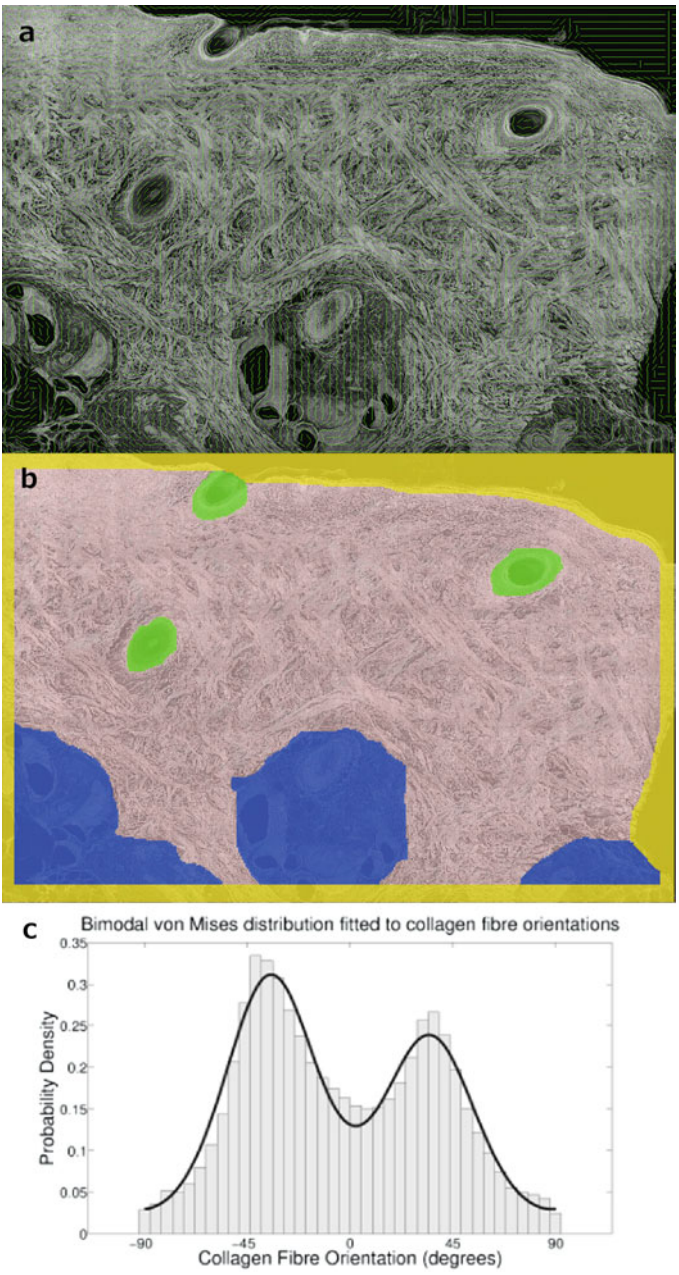

Fig. 8.5 Collagen orientation analysis: (**a**) A regular grid of computed fibre angles, using the structure tensor approach, shown as line segments; (**b**) Areas of the image containing non-collagenous structures, such as blood vessels, fat cells and glands, were masked out; (**c**) A mixture of two von Mises distributions fitted to collagen fibre orientations presented in the form of a histogram

were bi-modal for all sectioning orientations. To determine whether there was any difference in the collagen structure across the four different sectioning orientations, an analysis of variance (ANOVA) was performed on the fitted orientation means. It was shown that all p-values were greater than 0.05, indicating no significant differences in the fitted means across the four section orientation groups. The observations led to the proposal of a 3D conceptual model of collagen distribution for porcine skin, which will be described in the following section.

8.2.4 Conceptual Fibre Distribution Model

Based upon the observation of a lattice structure consistently observed in CLSM images of different sectioning orientations, it appears that porcine skin contains a rotationally symmetric 3D lattice structure about the normal direction to the epidermis. Thus, a 3D conceptual model to represent the observed collagen fibre distribution in porcine skin was proposed. Firstly, a material coordinate system (Fig. 8.6) was defined as follows: (1) N is normal to the epidermis; (2) L is parallel to the Langer's lines and (3) O is orthogonal to N and L.

Each fibre is defined in 3D space by its spherical coordinates $-\phi$ and θ (Fig. 8.6a). θ is the in-plane angle between L- and O-axes (with anti-clockwise defined as positive), whereas ϕ describes the fibre angle from the N-axis within the transverse section. It is assumed that the total probability of finding a fibre at

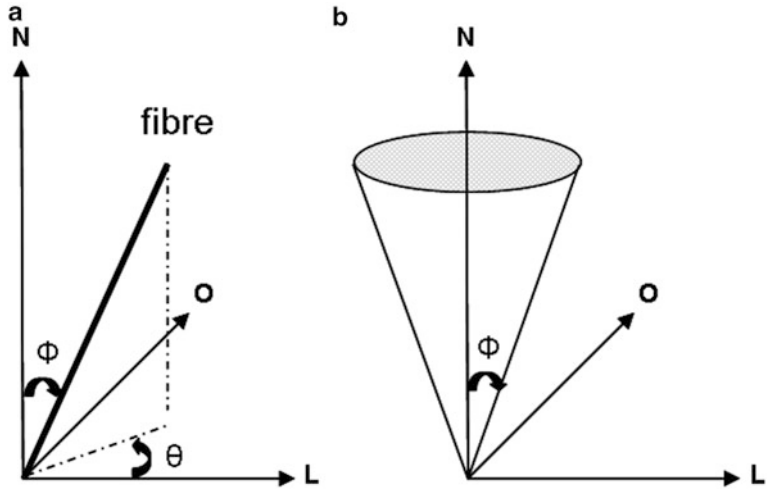

Fig. 8.6 3D conceptual model: (**a**) definition of a fibre with respect to the material coordinate system; (**b**) a circular distribution around the skin normal direction (N) is assumed based upon the similar collagen lattice network observed for the different sectioning orientations. L: Langer's line direction; O: direction orthogonal to N and L. Reproduced with permission from Jor et al. (2011b)

an orientation (ϕ,θ) can be determined by selecting appropriate density distribution functions $R_1(\phi)$ and $R_2(\theta)$ that independently represent ϕ and θ.

$$R(\phi, \theta) = R_1(\phi) \times R_2(\theta) \tag{8.8}$$

The in-plane angle θ describes structural information in the plane parallel to the epidermis. Although images acquired in this study do not provide any direct information, it is simplest to describe θ with a unimodal density distribution function, in which the fibre density in the direction of Langer's line has been observed to be greater than in any other direction. Cox (1941) showed that the preferred collagen orientation tends to be aligned along the Langer's lines. A unimodal π-periodic VM distribution, centred around the direction of Langer's lines, was chosen to describe the variation in θ.

For the idealised situation in which all the fibres are assumed to be perfectly aligned along two predominant orientations, the fibre distribution in the transverse planes may be represented by a rotationally symmetric distribution about the normal direction (Fig. 8.6b). This mathematical representation is consistent with the observations described in CLSM images of porcine skin collagen, i.e. that a similar lattice structure was apparent regardless of the sectioning orientation. Rather than being perfectly aligned, collagen fibres in biological tissues are likely to be dispersed about their mean directions within the lattice, thus requiring additional parameter(s) to describe the variation(s) about the predominant directions.

Based upon the bimodal nature of imaging data, a suitable density distribution function to describe ϕ is the mixture of two π-periodic VM distributions, defined as

$$R_1(\phi) = \frac{1}{2}\left(\frac{\exp\left[\kappa_{\phi_+}\cos(2(\phi - \mu_{\phi_+}))\right]}{\pi I_0(\kappa_{\phi_+})} + \frac{\exp\left[\kappa_{\phi_-}\cos(2(\phi + \mu_{\phi_-}))\right]}{\pi I_0(\kappa_{\phi_-})}\right) \tag{8.9}$$

where μ_ϕ and κ_ϕ are the mean and spread parameters, respectively, of the orientation distribution. As shown previously, both parameters can be directly estimated from analysis of CLSM images.

The total probability density function [Eq. (8.8)] is thus defined as the product of a unimodal VM distribution and a bimodal VM distribution to describe $R_1(\theta)$ and $R_2(\phi)$, respectively. By integrating the probability density function over the range $-\frac{\pi}{2} \leq \theta \leq \frac{\pi}{2}, -\frac{\pi}{2} \leq \phi \leq \frac{\pi}{2}$, all possible fibre orientations are covered by the unit hemisphere. Therefore, Eq. (8.8) must also satisfy the following normalisation constraint

$$\int_{\phi=-\frac{\pi}{2}}^{\frac{\pi}{2}} \int_{\theta=-\frac{\pi}{2}}^{\frac{\pi}{2}} R(\phi, \theta) d\theta d\phi = 1 \tag{8.10}$$

Consider a fibre in the reference configuration that is described by a vector $\mathbf{u}$. Since the stretch is identical in both the $+\mathbf{u}$ and $-\mathbf{u}$ directions, $R(\phi, \theta)$ must remain

invariant under the symmetrical transformation ($\phi \rightarrow \pi - \phi, \theta \rightarrow \pi + \theta$) for all values of ϕ and θ such that

$$R(\phi, \theta) = R(\pi - \phi, \pi + \theta) \tag{8.11}$$

In examining some commonly used statistical distributions, it was found that not all proposed distributions satisfied this physical restriction. For example, the commonly used unimodal Gaussian distribution does not satisfy Eq. (8.11).

Lokshin and Lanir (2009a) proposed a bimodal distribution in the form of trigonometric functions, given by

$$R(\theta) = c_{11}(\cos^4(\theta - \mu_\theta)) + c_{12}(\sin^4(\theta - \mu_\theta)) + \frac{c_2}{\pi} \tag{8.12}$$

where c_{11}, c_{12}, c_2 and μ_θ are constants. It can be seen that Eq. (8.12) satisfies the physical restriction for the planar angle θ. However, if the same distribution was used to represent ϕ, i.e.

$$R(\phi) = c_{11}(\cos^4(\phi - \mu_\phi)) + c_{12}(\sin^4(\phi - \mu_\phi)) + \frac{c_2}{\pi} \tag{8.13}$$

Equation (8.11) would not be satisfied.

In the proposed conceptual model, it can be shown that by choosing unimodal and bimodal VM distributions to describe $R_1(\theta)$ and $R_2(\phi)$, respectively, Eq. (8.8) satisfies the physical symmetry restriction. This is due to a factor of two in the θ distribution and the appearance of both $(\phi - \mu_\phi)$ and $(\phi + \mu_\phi)$ in the $R_2(\phi)$ distribution.

In this section, we have described techniques to mathematically represent tissue structure by combining confocal imaging and statistical analyses. Structural data in this form act as important inputs to structurally based constitutive models, which will be introduced in the following section.

8.3 Constitutive Modelling of Connective Tissues

The model-based approach, which uses finite element (FE) models to simulate the mechanical testing of tissues, provides an effective means to analyse rich sets of experimental data. This iterative numerical-experimental technique allows the identification of constitutive parameters. A selection of the constitutive models used in characterising the response of soft membranes will be presented here.

8.3.1 Phenomenological Models

Phenomenological models are mathematical functions, such as the power or exponential forms, that are chosen to best fit experimental data or reflect material behaviour. Based upon the classical biaxial testing of rabbit skin, Tong and Fung developed the widely used Fung constitutive equations for soft tissues (Fung 1965, 1967). In order to model the J-shaped stress–strain curves observed from the experiment data (i.e. a low stiffness region followed by an abrupt transition to a high stiffness region), the following generalised form was proposed:

$$\begin{aligned} W = & \frac{1}{2}(\alpha_1 E_{11}^2 + \alpha_2 E_{22}^2 + \alpha_3 E_{12}^2 + 2\alpha_4 E_{11} E_{22}) \\ & + \frac{1}{2} c \exp(a_1 E_{11}^2 + a_2 E_{22}^2 + a_3 E_{12}^2 + 2a_4 E_{11} E_{22} \\ & + \gamma_1 E_{11}^3 + \gamma_2 E_{22}^3 + \gamma_4 E_{11}^2 E_{22} + \gamma_5 E_{11} E_{22}^2) \end{aligned} \tag{8.14}$$

where α_i, a_i, γ_i and c are material constants and E_{ij} is the Green strain tensor, resulting in a total of 13 constitutive parameters. It was found by Tong and coworkers that Eq. (8.14) can be simplified by omitting the α_i and γ_i terms without compromising the goodness of fit to a majority of stress–strain curves. In biaxial testing, this equation can be further simplified by assuming the shear strain E_{12} is zero, thus can be written as

$$W = \frac{c}{2} \exp(a_1 E_{11}^2 + a_2 E_{22}^2 + 2a_4 E_{11} E_{22}) \tag{8.15}$$

While phenomenological models often provide good fits to experimental data, a major limitation of phenomenological models is that the constitutive parameters do not bear any physical meaning. Driven by the need to relate tissue behaviour to structure, structural constitutive models have since been developed and employed in studies to investigate soft tissue mechanics.

8.3.2 Structural Models

Structural models aim to formulate the constitutive relations based upon the underlying tissue histology. Since constitutive parameters relate to specific biological features, structural models are capable of providing insights into the important relationship between tissue structure and behaviour. Lanir (1979, 1983) was one of the first researchers to consider the geometric arrangement of fibre networks in soft connective tissues. Following his pioneering work, structurally based constitutive models have since been developed over the years for a variety of tissues such as arterial walls (Holzapfel et al. 2002), pericardium (Sacks 2003), tendon/ligament

(Hurschler et al. 1997), passive myocardium (Horowitz et al. 1988; Holzapfel and Ogden 2009) and heart valves (Billiar and Sacks 2000).

Recently, Lokshin and Lanir (2009a) presented an extensive approach to model the in vitro uniaxial response of membranous tissues. The effects of tissue nonlinearity, anisotropy, viscoelasticity, orientation and recruitment of two fibre networks (collagen and elastin), and preconditioning adaptations have been considered in a single constitutive model. The model, with 31 constitutive parameters, provided good fits to biaxial data of rabbit skin. An important outcome from this study was the investigation and incorporation of preconditioning effects in the experimental setting and constitutive models, respectively. Since different test protocols recruit different sets of fibres, the loading history (and hence preconditioning adaptation) will alter the time-dependent response of the tissue. It has been suggested that the underlying mechanisms are different for the two types of fibres: strain- and time-dependent increases in the reference length of collagen fibres, and strain-dependent strain softening (i.e. Mullins effect) of elastin fibres. The study also confirms the notion that the ground matrix and elastin contribute predominantly in the low strain regions, while collagen fibres are important for higher strains.

Representing Fibre Orientations with Continuous Distributions

Although a comprehensive constitutive description of soft tissue mechanics is desirable, the bottleneck is often the lack of ability to accurately identify the unknown constitutive parameters. The identification of constitutive parameters is a challenging task, even in the case of simple, isotropic and heterogeneous materials (Babarenda Gamage et al. 2011). Therefore, to characterise the biaxial response of porcine skin (outlined in the following section), we considered a simplified version of the structural model proposed by Lanir. In this micro-structural model, a network of collagen fibres with varying orientations is embedded in a tissue block consisting of ground matrix. The tissue block was assumed to be very small compared to the whole tissue, such that the material can be assumed to be homogeneous within each block and that the deformation field varies linearly over the block. The following assumptions were made:

- each fibre is undulated and only resists load when completely straightened.
- fibres can only resist tensile loading and buckle under compressive loads, i.e. no load is required to fold or unfold fibres.
- each fibre undergoes a uniaxial strain, which is representative of the macroscopic tissue strain along the fibre direction.
- the fibres are assumed to be linearly elastic when stretched, and their mechanical properties are governed by a one-dimensional (1D) fibre load-stretch relation.
- viscoelastic effects are ignored.

The second Piola–Kirchhoff stress tensor, $\mathbf{S}$, sums the contributions from the ground matrix $\mathbf{S}_m$ and collagen fibres $\mathbf{S}_f$, respectively, by taking into consideration the fibre volume fraction V_f, such that

$$\mathbf{S} = (1 - V_f) \cdot \mathbf{S}_m + V_f \cdot \mathbf{S}_f \tag{8.16}$$

The ground matrix is assumed to be an isotropic neo-Hookean material; thus, the strain energy function of the ground matrix (W_m) is given by

$$W_m = K_m(I_1 - 3) \tag{8.17}$$

where K_m is the stiffness of the ground matrix and I_1 is the first principal strain invariant of the Cauchy–Green deformation tensor. For a 2D membrane, the second Piola–Kirchhoff stress tensor for the ground matrix can be expressed as

$$S_{ij}^m = \frac{\partial W_m}{\partial E_{ij}} = \frac{\partial W_m}{\partial I_1}\frac{\partial I_1}{\partial E_{ij}} = \begin{cases} 2K_m & i = j \\ 0 & i \neq j \end{cases} \tag{8.18}$$

where $\mathbf{E}$ is the Green–Lagrange strain tensor. A uniaxial fibre strain energy function (w_f) is defined as a function of the fibre stretch ratio λ

$$w_f = \frac{K_c}{2}(\lambda - 1)^2 \tag{8.19}$$

where K_c is the collagen fibre stiffness and λ is given by Eq. (8.20).

$$\begin{aligned} \lambda &= \sqrt{2\gamma_f' + 1} \\ &= \sqrt{2(E_{11}\cos^2\theta + E_{22}\sin^2\theta + 2E_{12}\cos\theta\sin\theta) + 1} \end{aligned} \tag{8.20}$$

where γ_f' represents the strain along the fibre in the deformed configuration and θ is the in-plane fibre angle.

The load per unit undeformed cross-sectional area in the fibre is

$$f(\lambda) = \frac{\partial w_f(\lambda)}{\partial \lambda} = \begin{cases} K_c(\lambda - 1) & \lambda > 1 \\ 0 & \lambda \leq 1 \end{cases} \tag{8.21}$$

The total strain energy of all fibres in an undeformed volume unit, W_f, is given by

$$W_f = \int_\theta R(\boldsymbol{\theta}) \cdot w_f(\lambda)\mathbf{d}\theta \tag{8.22}$$

where R is the probability density function for the fibre orientation. The summation can be replaced by integrals if there is a large enough number of fibres in each direction.

For a 2D membrane, the second Piola–Kirchhoff stress tensor for the fibres can be expressed as

$$S_{ij}^f = \int_\theta R(\theta)\frac{1}{\lambda}\frac{\partial \gamma_f'}{\partial E_{ij}} \cdot \int_{x=1}^{\lambda} D(x) \cdot f\left(\frac{\lambda}{x}\right)\mathbf{d}x\mathbf{d}\theta \tag{8.23}$$

where x is the stretch required to straighten an undulated fibre and $D(x)$ is the probability density function for fibre undulation. Continuous distribution functions are used to represent the orientation of collagen fibres, with the most commonly used being the Gaussian (Lanir 1983) and von Mises distributions. A unimodal π-periodic von Mises distribution was chosen to describe the in-plane fibre orientation θ. For fibre undulation, commonly used continuous distribution functions include the Gaussian, beta, Lorentz function and log-logistic distribution function. For present purposes, a Gaussian distribution was used to describe fibre undulation:

$$D(x) = \frac{1}{\sqrt{2\pi}\sigma_x}\exp\left\{-\frac{(x-\mu_x)^2}{2\sigma_x^2}\right\} \tag{8.24}$$

where μ_x and σ_x are the mean and standard deviation of the undulation distribution, respectively.

It is important to note that the above structural model has many simplifications, such as the omission of the elastic fibre response and time effects. However, we will demonstrate in Sect. 8.5 that, even with such a simplified model, there remains significant challenges with material parameter identification.

Discretised Fibre Model

Flynn et al. (2011a) proposed a discretised fibre structural model for soft tissues comprising of six fibre bundles. In this model, each fibre bundle was aligned parallel to lines that pass through opposing vertices of a regular icosahedron. Each fibre bundle was assumed to consist of a single elastin fibre in parallel with a distribution of undulated collagen fibres. The total strain energy function of the six fibre bundle ensemble was given by

$$W = f(J) + \sum_{i=1}^{6} w_i[W_e(\lambda_i) + W_c(\lambda_i)] \tag{8.25}$$

where $f(J)$ denotes the response to compression, and $W_e(\lambda_i)$ and $W_c(\lambda_i)$ is the strain energy of the elastin fibre and undulated bundle of collagen fibres, respectively. The total strain energy of equally weighted elastin fibres was represented by a modified neo-Hookean material.

To represent the strain energy of undulated collagen fibres, a novel approach involving analytical expressions was adopted. This approach does not require numerical integration of continuous distribution functions and is thus more computationally efficient. Two simple distribution functions (a step and triangular function) for collagen undulation that yield analytical stress–strain expressions were investigated. It was found that the fibre stresses closely matched those calculated using the normal distribution function, indicating that a two-parameter step function is sufficient to model collagen fibre undulation. The proposed discrete fibre model was used to fit experimental data from various biaxial tensile tests. Although

providing relatively good fits, this model is limited by the fact that it does not guarantee a polyconvex formulation and it does not yield isotropic response when all of the weights w_i are equal.

In Sects. 8.2 and 8.3, we have established characterisation of tissue structure and introduced a selection of constitutive relations. The measurement of mechanical response relies on performing mechanical tests on the tissues of interest, which will be discussed in the next section.

8.4 Mechanical Experiments

Over the years, many research groups have attempted to characterise and quantify the mechanical functions of soft tissues by performing mechanical experiments. Two types of deformation are typically applied—loads parallel to the surface of the tissue (such as uniaxial, biaxial tension and torsion), or loads applied perpendicular to the surface (such as suction and indentation). In this section, we will present some of our recent instrumentation developments in measuring the mechanical response of skin tissues.

8.4.1 Biaxial Testing

Biaxial testing has been employed to determine the material properties of skin (Lanir and Fung 1974a,b), pericardium (Choi and Vito 1990; Billiar and Sacks 1997; Sacks 2003), lung parenchyma (Vawter et al. 1978) and thin sections of myocardium (Yin et al. 1987; Smaill and Hunter 1991; Humphrey et al. 1990). Prior to this, mechanical tensile tests were often restricted to uniaxial tests (Daly 1966; Manschot and Brakkee 1986) due to challenges in prescribing the appropriate boundary conditions. Biaxial testing presents many technical difficulties, including the need to control two boundary conditions, minimising gripping effects, applying forces uniformly along the specimen edge, and determining the optimal specimen size to promote homogeneity within the specimen while ensuring that the region of interest is located sufficiently far from the exterior edges (Sacks 2003). Lanir and Fung (1974a) were the first researchers to investigate the mechanical properties of planar soft tissue using biaxial testing. A rabbit skin specimen was mounted on the biaxial device in a trampoline-like manner at 68 attachment points using thin threads. The stress and strain states across the central region of interest were considered to be uniform. Tissue strain within this region was obtained by measuring the distance between pairs of lines marked on the specimen using video dimensional analysers. From the experimental data, it was observed that the skin tissues exhibited J-shaped directionally dependent stress–strain curves, highlighting nonlinearity and

anisotropic mechanical behaviour. An important observation is that the stress–strain curves were independent of strain rate for both the loading and unloading cycles, within the range tested.

A major challenge in characterising and comparing the mechanical response of soft connective tissues, such as skin and pericardium, is the significant inter-specimen structural variability that exists, particularly relating to the anisotropy of the tissues. To minimise the underlying structural variability across specimens, Sacks (2003) developed biaxial testing protocols that incorporated the use of the SALS technique described in Sect. 8.2. Using the SALS imaging technique, tissue specimens with a high degree of structural uniformity were selected for biaxial testing. This resulted in consistent mechanical response across specimens and low variability in the identified constitutive parameters. Rectangular samples of bovine pericardial specimens and porcine aortic valve leaflets were attached to the biaxial rig in the trampoline-like manner with sutures. To track the strain field, four graphite markers (∅0.3 mm) were attached to the central region of the specimen using cyanoacrylate adhesive. The positions of these markers were continuously tracked during deformation using a CCD camera. It was demonstrated that the use of SALS with biaxial testing provided additional insight into the relationship between fibre alignment and mechanical anisotropic behaviour.

In order to identify anisotropic, nonlinear, and inhomogeneous properties of soft membranes, it is necessary to subject the sample to a rich set of deformations, as will be described in Sect. 8.5.2. In addition, the use of a model-based approach provides a framework within which to interpret the acquired experimental data. To this end, our group has developed a novel biaxial tensile device that is capable of imposing rich sets of complex deformation fields.

Biaxial Rig Hardware

The biaxial tensile rig (Fig. 8.7a) consists of up to 16 displacement actuators (Physik Instrument DC-Mike, Germany) arranged in a circular array to stretch the tissue specimen (Nielsen et al. 2002). Since the movement of each motor axis is controlled independently, the circular arrangement permits a rich set of strains to be applied to the membrane. Each actuator, controlled by a Hewlett Packard HCTL100 motor controller, has a displacement range of 50 mm and position accuracy of 0.2 μm. The minimum specimen size is restricted by the radius at which transducers can converge without colliding. For the 16 axis set-up, the minimum diameter is 50 mm. A smaller specimen size of 20 mm can be accommodated by using eight transducers.

Mounted at the tips of each displacement actuator is a 2D force transducer that measures the forces applied to the membrane during testing. Each force transducer is made up of two pairs of strain gauges, arranged as two half-Wheatstone bridges, bonded to the four necked surfaces of a cantilever. They measure the strain applied to the surface of the cantilever when force is applied at the attachment pin. The membrane is attached to the transducers via a sharp needle at the end of a 30 mm long pin. This provides a quick and easy tethering method, compared with

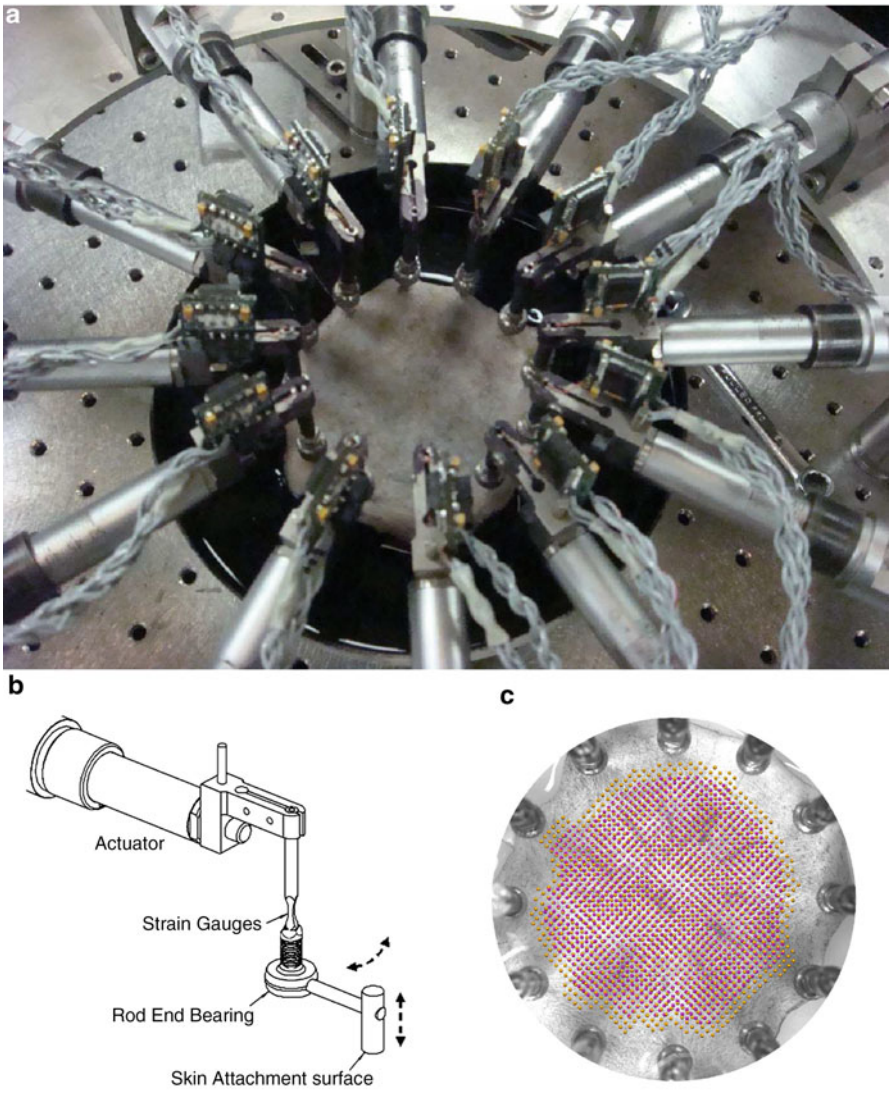

Fig. 8.7 Biaxial rig set-up: (**a**) Tensile tests were performed on in vitro samples of porcine skin bathed in phosphate buffered solution; (**b**) Alternative method of attaching in vivo samples to the biaxial rig using a rod end bearing approach; (**c**) Tracking of material points from the reference configuration to the deformed configuration. The CCD image of the deformed sample is shown in the background. Reproduced with permissions from Jor et al. (2011a) and Kvistedal and Nielsen (2009)

thin threads commonly used in biaxial devices. The deformed geometry and the associated deformed speckle pattern applied to the membrane surface are captured using a CCD camera (Atmel Corporation, France, Camelia 4 M). These images are used to compute the deformation field of the membrane using nonlinear cross-correlation techniques, which are described in the following section. The system uses a 12-bit monochrome camera with a 2048 pixel × 2048 pixel resolution. It is equipped with a bellows and an El-Nikkor (Tokyo, Japan) 80 mm enlarger lens, providing a field-of-view of 20–200 mm. The actuator control, force measurements, and image acquisition are controlled using an integrated software system developed with LabView (National Instruments).

Cross-Correlation Technique for Tracking Deformation

The measurement of strain fields poses a significant challenge in biaxial testing of soft biological tissues. Ideally, one would measure strain optically to avoid any mechanical interference. Malcolm et al. (2002) proposed a novel technique to measure the displacement of material points over the specimen using a phase-based cross-correlation technique, and subsequently compute the strain field via finite element modelling. The mathematics of this procedure have been previously described in detail by Malcolm (2000) and thus will only be briefly summarised here.

At each successive loading step, forces at the membrane boundary are recorded and an image of the speckled surface of the deformed specimen is acquired. In order to compute the displacement of a material point initially positioned at (x, y) in the undeformed configuration and later moved to $(x + \delta x, y + \delta y)$ using a phase-based Fourier transform cross-correlation (FTCC) method, signals with a wide spatial frequency bandwidth are required. In the biaxial testing set-up, this is achieved by applying a random speckle pattern on the surface of the membrane being tested. The FTCC method computes the 2D displacement vector of a region on the specimen when it is stretched from one state to another.

The total displacement is calculated by adding displacement obtained from the phase data to the displacement obtained by the amplitude data. This technique is capable of resolving displacements to a sub-pixel resolution (as small as 0.008 pixel). It is important to note that the cross-correlation gives the average displacement of the region within the subimage, and only works under the following conditions: (1) the visual pattern has a wide frequency bandwidth; (2) the displacement of the two subimages is relatively small compared with the size of the subimages, and; (3) there is little distortion or rotation associated with the deformation (i.e. deformation is homogeneous) within the subimage, although this can be accounted for using the underlying FE model.

To determine the strain field, a geometric FE geometric model of the undeformed membrane geometry is created and deformed to the measured displacements using least-squares fitting to obtain the geometric model of the deformed state. The deformation of the geometric model is used to compute the associated strain field.

Applications to Skin Tissues

The biaxial testing device was used to characterise the biaxial mechanical response of porcine skin (Jor et al. 2011a). For this experiment, a 12-transducer configuration was used to deform in vitro square samples (70 × 70 mm) of porcine skin excised along the abdominal mid-line of the animal. To determine the pretension, each sample was allowed to relax in phosphate buffered solution (PBS) over a period of 3–4 h (defined as the *unloaded* state). The changes in length along each of the 12 directions were estimated, by comparing an image of the sample in its unloaded and preloaded (i.e. in vivo or intact) states. In general, the skin samples retracted 40 % in the direction parallel to the torso mid-line (also the Langer's lines) and 20 % in the normal direction. Pretension forces were defined as the forces required to stretch a specimen from its unloaded to preloaded configuration. From the preloaded configuration, equi-axial deformations were imposed by stretching circular skin specimens uniformly along 12 directions using the biaxial rig, with the resultant loads at the membrane attachment points being measured. Displacement fields at each deformation step were tracked using the image 2D cross-correlation technique described above (Fig. 8.7c).

The biaxial rig has also been used to characterise the mechanical response of human forearm skin in vivo. Five healthy male subjects, between 29 years and 35 years of age, participated in this study (Kvistedal and Nielsen 2009). To avoid the use of fixed attachment points, which would lead to undesired vertical and torsional stresses in the sample, a miniature rod end bearing was used to attach the skin surface to the force transducers (Fig. 8.7b). Equi-axial deformations were imposed in increments of 0.2 mm along and across the Langer's lines of the forearm. Cross-correlation techniques were used to track the displacements between each successive loading state. It was observed that the stress–strain curves were different between individuals, further demonstrating variations in the mechanical properties of skin that is dependent on age, body locations and gender.

8.4.2 Three-Dimensional Testing

There are important limitations with biaxial testing of soft tissues. Researchers have commented on the inability to infer any in-plane shear information due to difficulties in imposing and controlling shear stresses in planar biaxial tests (Humphrey et al. 1990; Sacks 2000). Simple shear devices have been developed by Arbogast et al. (1997) and Dokos et al. (2000) for testing myocardial tissues, but these studies did not combine shear with biaxial stretching. Extension and inflation tests on tubular specimens, combined with torsion, have similar effects to planar biaxial tests with simple shear. The first experiment of this kind was performed by Humphrey et al. on cylindrical blood vessels (Humphrey et al. 1993). However, in order to completely characterise the 3D anisotropic mechanical response of soft tissues, an additional independent, out-of-plane deformation is required (Holzapfel and Ogden 2009).

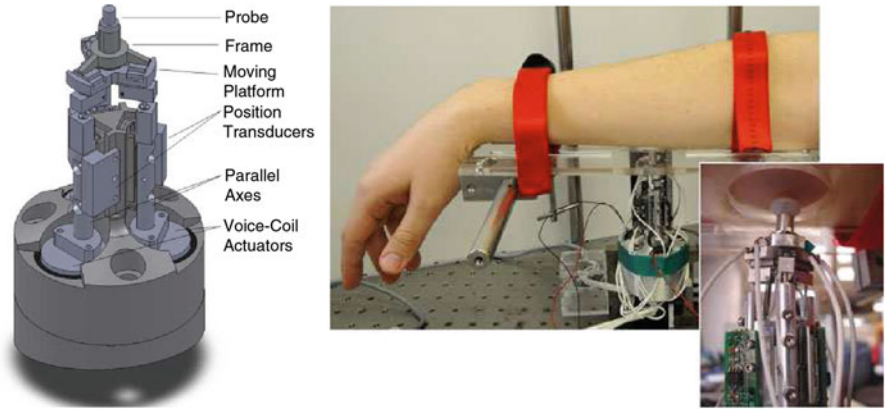

Fig. 8.8 Three-dimensional measurements using a force-sensitive micro-robot. Reproduced with permission from Flynn et al. (2011a)

To date, there is no biaxial device that will independently control and measure three components of stress or strain. In an attempt to impose a rich set of three-dimensional deformations on soft tissues, such as the skin, we have developed a novel force-sensitive micro-robot (Fig. 8.8).

Technical details of the micro-robot are provided in Flynn et al. (2011a) and will only be summarised here. The micro-robot consists of a 4-mm-cylindrical probe attached to three parallel axes, each driven by a voice-coil actuator to allow controlled movement of the probe tip within a working volume. Three linear position transducers are used to measure the displacement of each actuator. The displacement resolution is 50 μm with a repeatability of 60 μm. The 3D force vector at the probe tip can be computed from the force measured by three force transducers placed between each actuator and the probe, with a resolution of 6 mN with a repeatability of 8 mN. In a study to investigate the in vivo mechanical properties of human skin, 21 volunteers between the age of 21 and 52 years were recruited (Flynn et al. 2011a). To position the arm relative to the micro-robot, a plate with a 40 mm diameter hole was used to support and define the testing region.

A rich set of three-dimensional deformations was imposed, with a cycle frequency of 0.1 Hz, at three locations of the arm: the anterior right forearm; the anterior left forearm; and posterior right upper arm. Liquid cyanoacrylate adhesive was used to attach the micro-robot probe to the skin. The skin was preconditioned by performing three triangular-wave cycles. Firstly, in-plane deformations were applied, using 0° increments, in directions 0°–180° relative to the longitudinal axis of the arm. A series of out-of-plane deformations was then applied within planes oriented 0°, 45° and 90° relative to the longitudinal axis and normal to the surface of the arm. Normal indentations were also investigated. Results demonstrated that at all testing locations for all subjects, the skin exhibited nonlinear and anisotropic mechanical characteristics with significant hysteresis. Figure 8.9

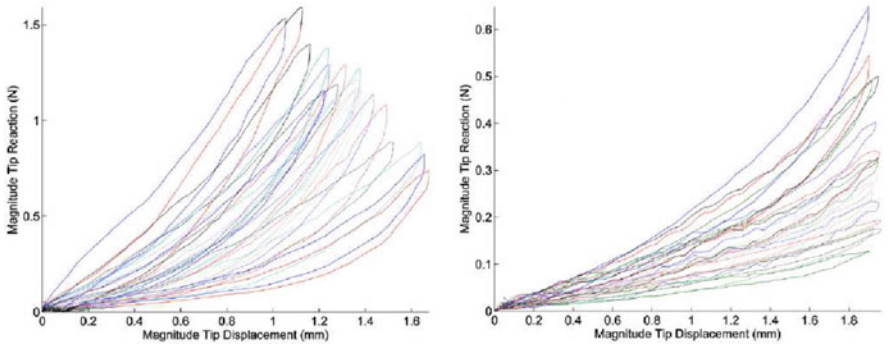

Fig. 8.9 Force-displacement curves of the anterior right forearm for all subjects tested subjected to in-plane (*left*) and out-of-plane (*right*) loading at 0° to the longitudinal axis of the arm. Reproduced with permission from Flynn et al. (2011a)

shows the force-displacement curves of the anterior right forearm for all subjects subjected to in-plane and out-of-plane loading at 0° to the longitudinal axis of the arm and normal deformations. Anisotropic effects cannot be quantified by experimental devices that apply torsion, suction or normal indentation deformations. This highlights a major advantage of the force-sensitive micro-robot, which is capable of characterising anisotropic effects by imposing both in-plane and out-of-plane deformations. There was also a wide range of variations reported across different subjects, suggesting the importance of acquiring experimental data from different body locations of a large population of individuals.

In order to interpret the experimental data, FE models coupled with appropriate constitutive relations are employed to identify constitutive parameters. In the following section, we will discuss the techniques and challenges associated with material parameter identification of soft tissues.

8.5 Constitutive Parameter Identification

Parameters of the constitutive relations chosen to describe skin are often determined by using model-based approaches where model predicted responses are fitted to experimental measurements obtained from devices such as those described in Sect. 8.4. This is usually performed using nonlinear optimisation techniques. Identifying these constitutive parameters for individual specific tissues can be valuable for determining normal vs pathological changes in a number of clinical applications. These include diagnosis of dermatological diseases, such as systemic scleroderma or other collagen related diseases, while also providing insight into improved clinical treatment and management of wounds and burns, where creation of skin scaffolds mimicking the behaviour of biological skin is required. However,

determining the optimal constitutive parameters is generally a non-trivial exercise since there are many factors which can potentially confound this process. These are issues related to the large number of parameters used to describe the stress–strain responses, many of which appear to tradeoff (or be correlated) when insufficient experimental data is available for identification. It is usually difficult to ascertain this information requirement prior to performing the experiments, which can lead to difficulties in identifying these parameters.

In previous studies, both phenomenological and structurally based constitutive relations have been extensively used for fitting to specific in vitro samples of human or animal tissue. In doing so, the descriptive power of the models has also been characterised by analysing the accuracy of the fit. One benefit of in vitro testing is the ability to finely control the experimental conditions, allowing the tissues to be subjected to specific modes of deformation such as uniaxial, biaxial and shear strains. This can help focus the identification to specific attributes of the tissue, such as the biaxial response without considering shear. Such simplifications have helped the identification process by reducing the number of parameters required to be estimated. However, testing tissues in this manner becomes difficult in vivo and via non-invasive means, as often required in a clinical setting. This is due to the fact that it is difficult, if not impossible, to independently apply specific modes of deformation in vivo rendering the simplifications used with in vitro experiments unusable. While still a challenging task, phenomenologically based relations typically contain relatively few parameters, which reduces the complexity of the problem. However, the determination of constitutive parameters for structurally based relations remains a difficult task due to the complex experimental protocols required for determining their parameters (e.g. determination of fibre orientation, spread and undulation). Further modelling considerations also need to be taken into account when modelling the skin in vivo, such as the state of pre-tension and the coupling of skin to the underlying tissues. As a consequence, very few in vivo applications currently make use of structural-based constitutive relations despite their parameters directly relating to tissue microstructure and being biologically meaningful.

In this section, we highlight challenges in identifying constitutive parameters and strategies our group has employed to approach these issues. We first discuss results that highlight the difficulties associated with identifying constitutive parameters of in vitro skin using the structurally-based model described in Sect. 8.3. Next we discuss a case study performed on synthetic materials which aimed to investigate the identification issues in closer detail and look at methods for improving identifiability. We then describe more recent studies which aim to characterise in vivo skin using non-invasive techniques. Issues regarding the pre-tension and time-dependent mechanical response of skin are also discussed.

8.5.1 *In Vitro Biaxial Testing of Skin*

This section summarises a study that was performed to identify the mechanical properties of porcine skin using the structurally based constitutive relation described in Sect. 8.2.1. A quasi-static modelling framework was developed to simulate the experiments described in Sect. 8.4.1, whereby measured forces were applied to FE models that were created to represent the geometry and structure of the tissue samples. Parameters of the structurally based constitutive relation, which were assumed to be homogeneous across the entire specimen, were identified using nonlinear least squares optimisation. The objective function to be minimised was the sum of squared errors between experimentally tracked material points on the skin surface (described in Sect. 4.1.3), and their corresponding points embedded in the model. The optimisation was subjected to box constraints describing physiologically appropriate upper and lower bounds for each constitutive parameter which are described in the next section.

Identification Strategy

Due to the large number of parameters in the constitutive relation described in Sect. 8.3, there appeared to be 'trade-off' effects for the optimisations, thus the number of estimated parameters was limited to subsets. In the identification procedure, two different estimation strategies were investigated, as listed in Table 8.1. The parameters to be identified for *Strategy A* were mean orientation (μ_θ), collagen stiffness (K_c) and matrix stiffness (K_m); for *Strategy B*, parameters were the mean orientation (μ_θ), mean undulation (μ_x) and matrix stiffness (K_m). The fixed parameters for both strategies were fibre orientation spread (κ), fibre undulation SD (σ_x) and volume fraction (V) and were set to values previously reported in the literature. Fibre spread κ was fixed to 10 (equivalent to a circular

Table 8.1 List of parameters for a 2D a structural constitutive relation with the corresponding lower/upper bounds and values from the literature ([a]Jor et al. 2011b; [b]Manschot 1985; [c]Viidik 1980)

Type	Parameter	Description	L.B.	U.B.	Strategy A	Strategy B
Structural	Fibre orientation θ	Mean μ_θ	0	π	Free	Free
		Spread κ_θ	–	–	Fixed at 10[a]	Fixed at 10[a]
	Fibre undulation x	Mean μ_x	1.0	1.8	Fixed at 1.2[b]	Free
		SD σ_x	–	–	Fixed at 0.2[b]	Fixed at 0.2[b]
	Volume fraction V		–	–	Fixed at 0.3[b]	Fixed at 0.3[b]
Non-structural	Fibre stiffness	K_c	0.3 MPa	500 MPa	Free	Fixed at 100 MPa[c]
	Ground matrix stiffness	K_m	1 kPa	100 kPa	Free	Free

SD of 21°) based upon quantitative analysis of collagen orientation in porcine skin (Jor et al. 2011b). In order to investigate the identifiability of the parameters, both estimation strategies were performed starting from ten different sets of initial estimates (random numbers generated between the lower and upper bounds for each parameter). Determinability criteria were also used to quantitatively assess parameter identifiability by analysing the Hessian matrix (i.e. the matrix of second partial derivatives of the objective function with respect to the model parameters) within the neighbourhood of the optimal set of parameters and are described further in Babarenda Gamage et al. (2011), Lanir et al. (1996), and Nathanson and Saidel (1985). These criteria were also used in subsequent studies in order to compare proposed identification strategies and improvements.

Results and Identifiability Issues

The optimal solutions for the samples, using *Strategy A* resulted in a matrix stiffness which ranged between 5 and 32 kPa. The mean orientations were similar across the three tissue samples, ranging between 167° and 178°, indicating that the mean fibre orientations deviated only 2°–13° from the torso midline. Collagen stiffness varied greatly across the three samples, ranging from 48 to 366 MPa. The reported range of collagen stiffness for tendons is also large, ranging from 100 MPa to 1.2 GPa (van Brocklin and Ellis 1965; Wright and Rennels 1964). The mean displacement errors of the optimal models using *Strategy A* ranged between 0.64 and 0.90 mm. For *Strategy B*, the optimal values for K_m and μ_θ were similar to those identified using *Strategy A*. The mean undulation at the optimum ranged from 1.04 to 1.34 across all samples. The mean displacement errors of the models optimised using *Strategy B* ranged between 0.63 and 1.03 mm.

Of the ten different sets of initial estimates used for *Strategy A*, only initial estimates with a mean orientation μ_θ relatively close to the optimal mean orientation converged to the same optimal solution for all tissue samples, regardless of large variations in the initial estimates of the other variable parameters (K_m and K_c). The initial estimates needed to be close to the optimal minimum to be found; thus, the identification problem was highly sensitive to μ_θ. Analysis of the identifiability of the parameters from the Hessian matrix obtained at the optimal set of parameters also reflected a high sensitivity to mean fibre orientation, confirming these observations. Similar observations were made for *Strategy B*, whereby the initial estimate for the mean orientation needed to be relatively close to the optimal mean orientation in order to achieve successful convergence. Although quantitative data on fibre orientation have been extracted from confocal images in a previous study as described in Sect. 8.2, this analysis was only performed on sagittal, not parallel, sections. Furthermore, although the samples used in imaging and mechanical experiments were excised from similar body locations of the pig, it would be better to use the same specimen for both imaging and experimental purposes in any future work in order to account for inter-specimen variations.

Given that the inter-specimen variability in structural arrangement may be large, fixing structural parameters such as fibre orientation spread, undulation mean, undulation spread, and fibre volume fraction of all the tissue samples to the same values (e.g. as reported in the literature) may potentially cause problems. In light of such difficulties in identifying parameters of the structural models, a case study was undertaken to help understand the general mechanisms leading to these identifiability issues and how they can be potentially mitigated.

8.5.2 Case Study: Highlighting Parameter Identification Issues

In order to investigate the identifiability issues in more detail, experiments were performed on silicone gel phantoms in Babarenda Gamage et al. (2011) under controlled conditions where boundary conditions and geometry of the body could be accurately prescribed. This allowed us to focus our attention solely on the identification problem. The study involved creating a two-layered cantilever structure from silicone gel ($70 \times 30 \times 30$ mm). Eight different gravity loaded orientations of the beam digitised using a FaroArm Laser ScanArm V2[1] and a tilt table. These datasets were used to assess both the descriptive and predictive power of the constitutive parameters of the beam that were subsequently identified using a similar model based identification approach as previously described.

Modelling

The two layers of silicone gel were modelled using an ideally incompressible hyperelastic neo-Hookean constitutive relation ($\Psi = c(I_1 - 3)$, where I_1 is the first invariant of the right Cauchy–Green deformation tensor). The different layers of the cantilever beam were described by two different stiffness parameters, c_a and c_b in units of kPa. These mechanical parameters were identified using an optimization method similar to that described in Sect. 8.5.1, however, in this case, the objective function was constructed from the laser scanned data using a closest point to model surface projection approach. The objective function to be minimised was defined as $\Phi = \sum_{j=1}^{M} \sum_{i=1}^{N_j} \|Z_{ij}\|^2$, where $\|Z_{ij}\|$ was the Euclidean distance between the i^{th} datapoint and its closest point on the surface of a model in experiment j, M is the number of experiments performed and N_j is the number of laser scanned data points in experiment j. In order to aid interpretation of the results, the root mean square error (RMSE) was used as defined in Eq. (8.26).

[1]Manufactured by FARO Swiss Holding GmbH, Switzerland: http://www.faro.com.

$$\text{RMSE} = \sqrt{\frac{\sum_{j=1}^{M}\sum_{i=1}^{N_j}\|Z_{ij}\|^2}{\sum_{j=1}^{M}N_j}} \tag{8.26}$$

The optimisation tolerance on the parameters was set to the nearest 1 Pa while the objective function tolerance was lowered to an RMSE value equivalent to 1e−9 mm.

Results

Figure 8.10 illustrates the optimal model fits to the experimental surface data and their associated parameter estimates when each orientation was analysed independently. The results show that even for this simple two-layered model, the stiffness parameters derived from individual experiments varied over a wide range of values even though the surface fitting errors were similar. Figure 8.11 illustrates how the use of one of these parameter sets to predict the deformations for the other orientations resulted in large surface fit errors.

A cross-validation study was performed to see whether the use of multiple orientations would improve the predictive power of the identified parameters.

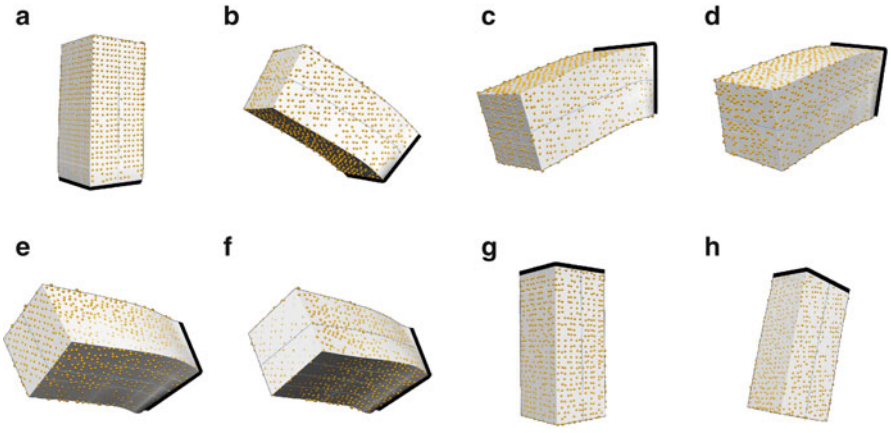

Fig. 8.10 Laser scanned datapoints from the eight cantilever beam orientations overlaid with best fit mechanics models using optimal stiffness parameters (indicated, in kPa) derived from individual gravity loading experiments. The fixed end of each model is indicated by a *thick outline*. It should be noted that model 1 (**a**) is orientated upright while model 7 (**g**) is orientated downward in the direction of gravity. Reproduced with permission from Babarenda Gamage et al. (2011). (**a**) Model 1: 1.82, 1.46 (**b**) Model 2: 4.72, 1.92 (**c**) Model 3: 4.37, 1.93 (**d**) Model 4: 4.57, 1.93 (**e**) Model 5: 4.79, 1.84 (**f**) Model 6: 4.13, 2.04 (**g**) Model 7: 4.91, 2.82 (**h**) Model 8: 3.70, 3.45

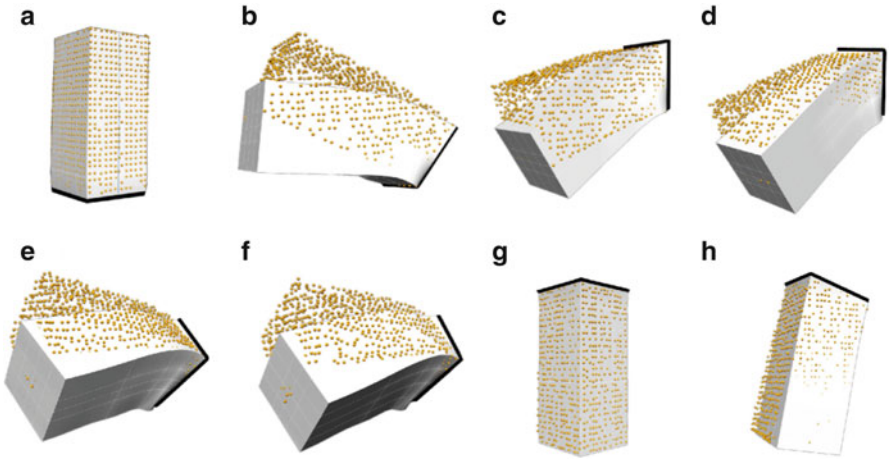

Fig. 8.11 Laser scanned data from the eight gravity loading experiments overlaid with predictions from models that used stiffness parameters derived from the upright orientation shown in Fig. 8.10. The maximum RMSE at the four corner points at the free ends of each beam was between 7.91 and 20.13 mm, respectively. Reproduced with permission from Babarenda Gamage et al. (2011). (**a**) Model 1 (**b**) Model 2 (**c**) Model 3 (**d**) Model 4 (**e**) Model 5 (**f**) Model 6 (**g**) Model 7 (**h**) Model 8

The cross-validation involved optimising a training subset of models against their respective experimental data. The resulting parameters were then used to estimate how accurately they could predict the deformation of the remaining validation subsets. The results were split into four groups, with groups 1 to 4 using 1, 2, 3 and 7 training models for identification, respectively, with eight sets of training models sampled randomly for groups 2 and 3 (for groups 1 and 4, all eight training sets were considered).

Visual interpretations of the results from groups 1 to 4 are presented in Fig. 8.12a–d, respectively, which show contour plots on the hyper-surfaces of the RMSE objective function. These hyper-surfaces were created by evaluating the objective function on the material parameter space. The markers on these plots indicate the optimal solution for each training set of models, which is the point at which the determinability of the parameters were also evaluated. The contours were plotted such that any set of parameters θ, which results in RMSE values less than γ, were inside the contour. For each contour, the value of γ was set to the optimal RMSE plus 0.1 mm to account for experimental error. Any pair of stiffness parameters inside this region can be considered as an equally valid solution within the limit of experimental error. The cross validation results showed that by increasing the number of training models used for parameter identification, the maximum RMSE error of the validation sets was reduced. The results also showed that we can satisfactorily estimate the stiffness properties of the two layers of the gel using three orientations with a maximum predictive RMSE of approximately 0.6 mm and maximum free corner error of approximately 1.9 mm. Some points

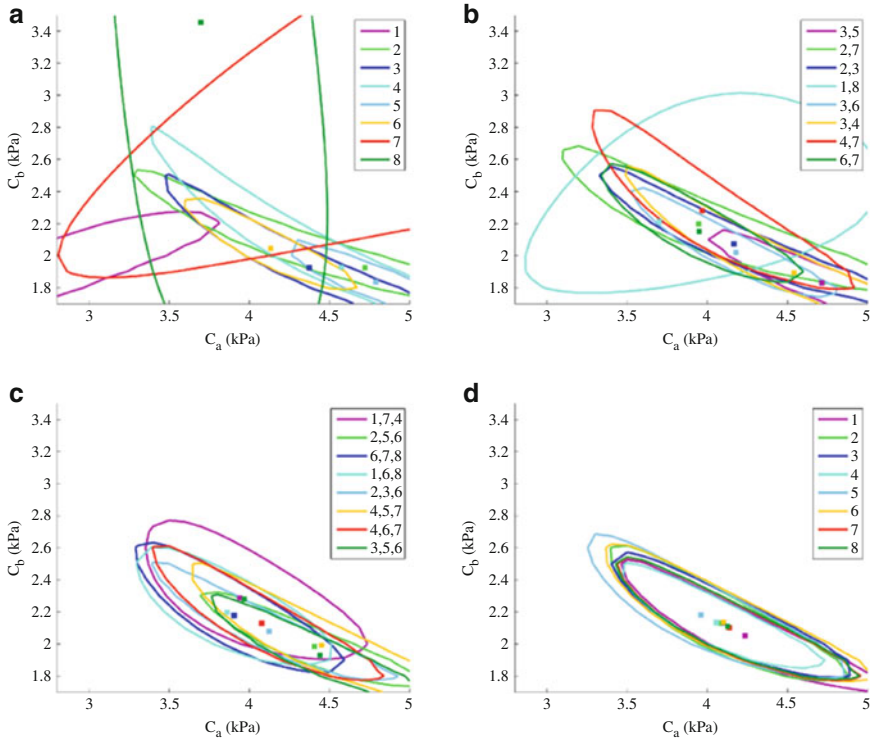

Fig. 8.12 Contour plots of the objective function (RMSE) over the stiffness parameter spaces. Panels (**a**) to (**d**) show contours as the number of training cases was increased from 1 to 2, 3 and 7, respectively, with legends indicating experiments included in the training sets (Groups 1–3), or the excluded experiment (Group 4). Areas where contours overlap represent parameter combinations that provide equally accurate predictions to within the experimental error. Reproduced with permission from Babarenda Gamage et al. (2011). (**a**) Group 1 (identification based on 1 model) (**b**) Group 2 (identification based on 2 models) (**c**) Group 3 (identification based on 3 models) (**d**) Group 4 (identification based on 7 models)

of interest related to the identification process, such as the uniqueness of the parameter estimates, are described in the following section, along with suggestions on techniques that could be used to further improve parameter identification.

Uniqueness of Parameter Estimates and Improving Identifiability

This study showed that choice of the optimality tolerance of the objective function affects the apparent uniqueness of the constitutive parameter estimates. Ideally, the optimisation should be terminated once the change in the objective function is less than the maximum error observed in the experimental measurements since this is the smallest physical quantity that can be accurately measured. Any optimisation solution which terminates under this condition should be valid (inside the contours in Fig. 8.12a–d). This gives rise to multitude of parameters sets, each of which is

an equally valid solution to the identification problem. Some of these solutions can give rise to a variety of prediction errors that depend upon where the true minimum lies. This can occur if the deformation is relatively insensitive to the constitutive parameters in certain orientations, as was the case for some of the models considered here, and noise in the data could easily shift the global optimum. Thus, some model's parameter estimates appeared as outliers, but in fact were valid solutions within the experimental accuracy. Another factor that can lead to non-unique solutions is the mathematical formulation of the constitutive relation and whether the parameters of the model are correlated. However, in this study, a single parameter was used to describe the stiffness of each layer of the beam and therefore any apparent correlation between the parameters was directly related to the information contained within the data.

Setting the objective function tolerance to a very low value during the identification procedure allowed the optimisation to terminate once the constitutive parameters converged to the nearest Pa. This resulted in unique solutions being obtained independent of the initial estimate. For this reason the optimal solutions provided in Fig. 8.10 (shown as markers) are only indicative of possible sets of valid parameters. However, the prediction results when the number of orientations used for identification was increased produced contours that overlapped to a greater extent. This reduced the possibility of obtaining parameters that would cause the large prediction errors seen in Fig. 8.11. It should be noted that with constitutive equations with a large number of unknowns, and a given dataset from which these parameters are required to be identified, it may not be possible to obtain unique solutions by lowering the tolerance on the optimised parameters (Ogden et al. 2004), especially if there is high correlation between parameters. This is related to the information content present within the data used to construct each model's objective function and whether this provides sufficient information for unique identification. For example, in this study, multiple solutions could potentially be produced with the two-layered cantilever beam if data from only one side of the beam was used for identification. This underscores the importance of the quality and quantity of the data that is used for fitting. High quality data would result in a smaller region in which parameters could equally well describe the model; while a rich set of data used for fitting the model would result in parameters which increase the ability of the models to predict different deformations.

The identification methodology for assessing and improving identifiability described in this section was used in our more recent studies looking at determining mechanical properties of skin in vivo. The results of these studies will be summarised in the next section.

8.5.3 In Vivo Identification of Skin Properties

Previous studies from our group have focussed on identifying constitutive parameters for a simplified form of the Tong and Fung strain energy function using

the biaxial rig on human forearm skin in vivo (Kvistedal and Nielsen 2009). This was achieved using a similar modelling and identification methodology as that described earlier in the previous sections. A series of multiaxial loading experiments were performed on the forearms of four age and gender matched subjects. The tissue geometry, together with recorded displacements and boundary forces, was combined with a nonlinear FE anisotropic membrane model to identify the mechanical parameters of the simplified Tong and Fung relation. Ten sets of constitutive parameters were estimated from the experiments and showed considerable differences in mechanical behaviour, both between individual subjects and symmetric locations on the body for a single subject. Variations between individuals have previously been reported as being dependent on body locations and age (Reihsner et al. 1995). The study showed that differences in the stress–strain relationship are also expected in identical body locations from age and gender matched subjects.

More recent studies from our group have utilised a micro-robot indenter (described in Sect. 8.4.2) for identifying mechanical parameters of human forearm skin. One such study will be described here, where the constitutive parameters of the Ogden and Tong and Fung constitutive models together with in vivo tensions were identified using a model-based approach (Flynn et al. 2011b). Based on the experiments on the silicon gel phantoms described in the previous section, it was shown that multiple loading conditions were important for improving identifiability of the constitutive parameters. We therefore aimed to obtain a rich set deformations, using the micro-robot indenter on the forearm for a number of volunteers, to aid subsequent identification and these are described in more detail in Sect. 8.4.2. The deformations included various in-plane and out-of-plane measurements of the force vs displacement response of the skin measured on the anterior forearm and posterior upper arm. Constitutive parameters were then identified from volunteers within this database using a model-based approach. To date, few finite element models in the literature have considered the effects of the in vivo pretension of the skin. In our studies, pretension was represented by an initial stress field imposed on the reference configuration in the X and Y directions, whereby the two parameters of the stress field were included in the optimisation procedure. When using only in-plane average forearm data to form the objective function, both the Tong and Fung and Ogden models provided good fits to the experimental data, with fitting errors of 9.9 and 11.6 %, respectively. However, they were unable to accurately predict the out-of-plane responses with overall fitting errors of 19.8 and 23.2 %, respectively. Using only the out-of-plane data in parameter optimisation, the Ogden model predicted the in-plane response with a fitting error of 17 %. The results from this study support the hypothesis that in-plane deformations alone do not provide sufficient data to identify the constitutive parameters and in vivo tensions. This hypothesis is further supported by the fact that increasing the number of deformation orientations leads to consistent improvements of the determinability criteria. It was also shown that there is a wide variability in parameter and predicted pre-stress values across the subjects, indicating the need to collect experimental data from a diverse population. A common problem in parameter estimation, especially when phenomenological

models are used, is the ability to address the issue of uniqueness of the optimal solution. A limitation of this study was the use of only the force and displacement measures on the tip of the microrobot for identifying the mechanical properties.

8.6 Conclusions and Outlook

Building upon the pioneering work of Professor Yoram Lanir, increasing research efforts over the years have now resulted in a well-established structurally based constitutive modelling framework for soft connective tissues. The present article has focused on some of the work by the Auckland Bioengineering Institute contributing towards the goal of understanding the structure–function relationship of soft membranous tissue. Key aspects of our work are to (1) develop constitutive relations based on quantitative information of tissue structure; and (2) use rich sets of experimental data to aid in accurate and reliable constitutive parameter identification.

To this end, we have developed imaging techniques to analyse collagen fibre networks and represent fibre orientations with mathematical distributions. Currently, there remains a shortage of quantitative structural data that can be directly incorporated into constitutive modelling frameworks, which will help reduce the number of constitutive parameters to be identified. It has also been demonstrated in one of our studies that a priori knowledge of mean fibre orientation is important to the success of parameter identification. Due to the high inter-specimen variability in soft tissues, it is highly desirable to extract both the structural and experimental data from the *same* tissue sample. However, this becomes difficult when in vivo tissues are of interest as invasive methods, such as conventional microscopy, can no longer be considered. To address this issue, work is currently underway in our group to develop alternative methods for gathering structural data in a non-invasive manner. Furthermore, although previous research effort has been primarily devoted to the studies of collagen fibre orientations, it is important to also understand the properties and interactions of other tissue constituents, such as elastin.

The use of complex structural constitutive models—which consider the effects of anisotropy, nonlinearity, viscoelasticity, preconditioning, and multiple families of fibres—relies heavily upon the availability of rich sets of experimental data. There is clearly a need to further improve current instrumentation techniques to achieve a wide range of deformation modes. In this article, we summarised the development of a multi-axial tensile device coupled with digital image correlation techniques to track the deformation field, used to characterise the planar stress–strain response of soft tissues. Since biaxial testing does not provide a complete 3D mechanical description, a force-sensitive micro-robot has been developed to impose out-of-plane deformations. It is expected that the measurement of the strain field in the vicinity surrounding the indenter probe, using digital image correlation techniques, would improve the identification of the constitutive parameters. In light of this, we are currently investigating techniques to obtain strain measurements by tracking

surface deformations using a 3D stereoscopic system (Alvares 2009; Evans and Holt 2009). In order to improve the identifiability of constitutive parameters, the design of optimal experiments (Humphrey 2003; Lanir et al. 1996) requires further development.

The merits of structurally based constitutive modelling frameworks becomes particularly apparent when the mechanics of ageing or diseased tissues are of interest. Structural changes in the microscopic level associated with ageing include the thickening of collagen fibres (which take on a much denser and sheet-like arrangement), and the fragmentation and aggregation of elastin fibres. Such geometric and mechanical changes in the individual tissue constituents are thought to contribute to the reduced extensibility and elasticity often observed in ageing skin. In order to gain improved understanding of the underlying mechanisms, structural models allow one to perturb structural constitutive parameters that are associated with time or pathological changes, and subsequently, predict the associated mechanical response. To be useful in a clinical setting, patient-specific computational models are likely to require the combination of fast and non-invasive image techniques, along with in vivo experimental data under various loading conditions.

Although recent research advancements have contributed to improved understanding of soft tissue biomechanics, many aspects of the complex interactions between microscopic structure and macroscopic mechanical response are still to be elucidated.

References

Abrahams M. Mechanical behaviour of tendon in vitro. Med Biol Eng Comput. 1967;5:433–43.

Alvares D. A 3D strain measurement system for soft materials: application to material parameter estimation. Master's Thesis, The University of Auckland; 2009.

Arbogast KB, Thibault KL, Scott Pinheiro B, Winey KI, Margulies SS. A high-frequency shear device for testing soft biological tissues. J Biomech. 1997;30(7):757–9.

Babarenda Gamage TP, Rajagopal V, Ehrgott M, Nash MP, Nielsen PMF. Identification of mechanical properties of heterogeneous soft bodies using gravity loading. Int J Numer Methods Biomed Eng. 2011;27(3):391–407.

Billiar K, Sacks M. A method to quantify the fiber kinematics of planar tissues under biaxial stretch. J Biomech. 1997;30(7):753–6.

Billiar K, Sacks M. Biaxial mechanical properties of the native and glutarldehyde-treated aortic valve cusp: part II - a structural constitutive model. J Biomech Eng. 2000;122:327–35.

Brown IA. A scanning electron microscope study of the effects of uniaxial tension on human skin. Br J Dermatol. 1973;89(4):383–93.

Carton RW, Dainauskas J, Clark JW. Elastic properties of single elastic fibers. J Appl Physiol. 1962;17(3):547–51.

Choi HS, Vito RP. Two-dimensional stress-strain relationship for canine pericardium. J Biomech Eng. 1990;112(2):153–9.

Cox H. The cleavage lines of the skin. Br J Surg. 1941;29(114):234–40.

Craik JE, McNeil IRR. Histological studies of stressed skin. In: Biomechanics and related bioengineering topics. Oxford: Pergamon Press; 1964. p. 159–64.

Daly C. The biomechanical characteristics of human skin. Ph.D. Thesis. Scotland: University of Strathclyde; 1966.

Daly CH. The role of elastin in the mechanical behavior of human skin. In: 8th International Conference on Medical and Biological Engineering; 1969.
Dokos S, LeGrice IJ, Smaill BH, Kar J, Young AA. A triaxial-measurement shear-test device for soft biological tissues. J Biomech Eng. 2000;122(5):471–8.
Dolber P, Spach M. Conventional and confocal fluorescence microscopy of collagen fibers in the heart. J Histochem Cytochem. 1993;41(3):465–9.
Eckert C, Mikulis B, Gottlieb D, Gerneke D, LeGrice I, Padera R, Mayer J, Schoen F, Sacks M. Three-dimensional quantitative micromorphology of pre- and post-implanted engineered heart valve tissues. Ann Biomed Eng. 2011;39:205–22.
Evans S, Holt C. Measuring the mechanical properties of human skin in vivo using digital image correlation and finite element modelling. J Strain Anal Eng Des. 2009;44:337–45.
Finlay B. Scanning electron microscopy of the human dermis under uni-axial strain. Biomed Eng. 1969;4(7):322–7.
Flynn C, Taberner A, Nielsen P. Measurement of the force-displacement response of in vivo human skin under a rich set of deformations. Med Eng Phys. 2011a;33(5):610–9.
Flynn C, Taberner A, Nielsen P. Modeling the mechanical response of human skin under a rich set of deformations. Ann Biomed Eng. 2011b;39:1935–46.
Freed AD, Einstein DR, Vesely I. Invariant formulation for dispersed transverse isotropy in aortic heart valves: an efficient means for modeling fiber splay. Biomech Model Mechanobiol. 2005;4(2–3):100–17.
Fung Y. Foundations of solid mechanics. Englewood Cliffs: Prentice-Hall; 1965.
Fung YC. Elasticity of soft tissues in simple elongation. Am J Physiol. 1967;213(6):1532–44.
Gasser TC, Ogden RW, Holzapfel GA. Hyperelastic modelling of arterial layers with distributed collagen fibre orientations. J R Soc Interface. 2006;3(6):15–35.
Harkness ML, Harkness RD. Effect of enzymes on mechanical properties of tissues. Nature. 1959;183:1821–2.
Holzapfel G, Ogden R. On planar biaxial tests for anisotropic nonlinearly elastic solids. a continuum mechanical framework. Math Mech Solids. 2009;14:474–89.
Holzapfel G, Gasser T, Stadler M. A structural model for the viscoelastic behavior of arterial walls: continuum formulation and finite element analysis. Eur J Mech A Solids. 2002;21:441–63.
Horowitz A, Lanir Y, Yin FCP, Perl M, Sheinman I, Strumpf RK. Structural three dimensional constitutive law for the passive myocardium. J Biomech Eng. 1988;110:200–07.
Humphrey J. Review paper: continuum biomechanics of soft biological tissues. Proc R Soc Lond A Math. 2003;459(2029):3–46.
Humphrey JD, Strumpf RK, Yin FCP. Determination of a constitutive relation for passive myocardium: I. A new functional form. J Biomech Eng. 1990;112(3):333–9.
Humphrey J, Kang T, Sakarda P, Anjanappa M. Computer-aided vascular experimentation: a new electromechanical test system. Ann Biomed Eng. 1993;21:33–43.
Hurschler C, Loitz-Ramage B, Vanderby R. A structurally based stress-stretch relationship for tendon and ligament. J Biomech Eng. 1997;119(4):392–9.
Jahne B. Practical handbook on image processing for scientific and technical applications, chap 13. 2nd ed. Boca Raton: CRC Press; 2004. p. 419–42.
Jor J, Nash M, Nielsen P, Hunter P. Estimating material parameters of a structurally based constitutive relation for skin mechanics. Biomech Model Mechanbiol. 2011a;10:767–78.
Jor JWY, Nielsen PMF, Nash MP, Hunter PJ. Modelling collagen fibre orientation in porcine skin based upon confocal laser scanning microscopy. Skin Res Tech. 2011b;17(2):149–59.
Junquiera LC, Montes GS, Sanchez EM. The influence of tissue section thickness on the study of collagen by the picrosirius-polarization method. Histochemistry. 1982;74:153–6.
Kenedi R, Gibson T, Daly C. Bio-engineering studies of the human skin: the effects of uni-directional tension. In: Structure and function of connective and skeletal tissue. London: Butterworths; 1965. p. 388–95.
Kvistedal YA, Nielsen PMF. Estimating material parameters of human skin *in vivo*. Biomech Model Mechanobiol. 2009;8(1):1–8.

Lanir Y. A structural theory for the homogeneous biaxial stress-strain relationships in flat collagenous tissues. J Biomech. 1979;12(6):423–36.
Lanir Y. Constitutive equations for fibrous connective tissues. J Biomech. 1983;16(1):1–12.
Lanir Y, Fung YC. Two-dimensional mechanical properties of rabbit skin. I. Experimental system. J Biomech. 1974a;7(1):29–34.
Lanir Y, Fung YC. Two-dimensional mechanical properties of rabbit skin. II. Experimental results. J Biomech. 1974b;7(2):171–82.
Lanir Y, Lichtenstein O, Imanuel O. Optimal design of biaxial tests for structural material characterization of flat tissues. J Biomech Eng. 1996;118:41–7.
Lokshin O, Lanir Y. Micro and macro rheology of planar tissues. Biomaterials. 2009a;30:3118–27.
Lokshin O, Lanir Y. Viscoelasticity and preconditioning of rat skin under uniaxial stretch: microstructural constitutive characterization. J Biomech Eng. 2009b;131(3):031009.
MacKenna DA, Omens JH, Covell JW. Left ventricular perimysial collagen fibers uncoil rather than stretch during diastolic filling. Basic Res Cardiol. 1996;91(2):111–22.
Malcolm D. Estimating the material properties of inhomogeneous elastic membranes. Ph.D. Thesis, University of Auckland; 2000.
Malcolm DTK, Nielsen PMF, Hunter PJ, Charette PG. Strain measurement in biaxially loaded inhomogeneous, anisotropic elastic membranes. Biomech Model Mechanobiol. 2002;1: 197–210.
Manschot JFM. The mechanical properties of human skin *In Vivo*. Ph.D. Thesis. The Netherlands: Nijmegen University; 1985.
Manschot JF, Brakkee AJ. The measurement and modelling of the mechanical properties of human skin *in vivo*–I. The measurement. J Biomech. 1986;19(7):511–5.
Marcarian HQ, Calhoun ML. Microscopic anatomy of the integument of adult swine. Am J Vet Res. 1966;27(118):765–62.
Meijer R. Characterisation of anisotropic and non-linear behaviour of human skin. Technical Report, Personal Care Institute of Philips Research Laboratories; 1997.
Melis P, Noorlander ML, van der Horst CMA, van Noorden CJF. Rapid alignment of collagen fibers in the dermis of undermined and not undermined skin stretched with a skin-stretching device. Plast Reconstr Surg. 2002;109(2):674–82.
Meyer W, Neurand K, Radke B. Collagen fibre arrangement in the skin of the pig. J Anat. 1982;134:139–48.
Mowafy M, Cassens RG. Microscopic structure of pig skin. J Anim Sci. 1975;41(5):1281–90.
Nathanson MH, Saidel GM. Multiple-objective criteria for optimal experimental design: application to ferrokinetics. Am J Physiol. 1985;248:378–86.
Nielsen PMF, Malcolm DTK, Hunter PJ, Charette PG. Instrumentation and procedures for estimating the constitutive parameters of inhomogeneous elastic membranes. Biomech Model Mechanobiol. 2002;1(3):211–8.
Noorlander ML, Melis P, Jonker A, van Noorden CJF. A quantitative method to determine the orientation of collagen fibers in the dermis. J Histochem Cytochem. 2002;50(11):1469–74.
Ogden RW, Saccomandi G, Sgura I. Fitting hyperelastic models to experimental data. Comput Mech. 2004;34(6):484–502.
Pope AJ, Sands GB, Smaill BH, LeGrice IJ. Three-dimensional transmural organization of perimysial collagen in the heart. Am J Physiol-Heart C. 2008;295(3):1243–52.
Reihsner R, Balogh B, Menzel EJ. Two-dimensional elastic properties of human skin in terms of an incremental model at the *in vivo* configuration. Med Eng Phys. 1995;17(4):304–13.
Sacks M. Biaxial mechanical evaluation of planar biological materials. J Elast. 2000;61:199–246.
Sacks MS. Incorporation of experimentally-derived fiber orientation into a structural constitutive model for planar collagenous tissues. J Biomech Eng. 2003;125(2):280–7.
Sacks M, Smith DB, Hiester E. A small angle light scattering device for planar connective tissue microstructural analysis. Ann Biomed Eng. 1997;25:678–89.
Sands GB, Gerneke DA, Hooks DA, Green CR, Smaill BH, LeGrice IJ. Automated imaging of extended tissue volumes using confocal microscopy. Microsc Res Tech. 2005;67(5):227–39.

Sands G, Goo S, Gerneke D, LeGrice I, Loiselle D. The collagenous microstructure of cardiac ventricular trabeculae carneae. J Struct Biol. 2011;173(1):110–6.

Silver F, Kato Y, Ohno M, Wasserman A. Analysis of mammalian connective tissue: relationship between hierarchical structures and mechanical properties. J Long Term Eff Med Implants. 1992;2(2–3):165–98.

Smaill B, Hunter P. Structure and function of the diastolic heart. In: Theory of heart: biomechanics, biophysics, and nonlinear dynamics of cardiac function. New York: Springer; 1991. p. 1–29.

Spurr BD, Koutbeiy MA. A comparison of various methods for estimating the parameters in mixtures of von mises distributions. Commun Stat Simul Comput. 1991;20:725–42.

Sweat F, Puchtler H, Rosenthal SI. Sirius red f3ba as a stain for connective tissue. Arch Pathol. 1964;78:69–72.

Tong P, Fung YC. The stress-strain relationship for the skin. J Biomech. 1976;9(10):649–57.

van Brocklin D, Ellis DG. A study of the mechanical behavior of toe extensor tendons under applied stress. Arch Phys Med Rehabil. 1965;46:369–73.

van Zuijlen P, Ruurda J, van Veen H, van Marle J, van Trier A, Groenevelt F, Kreis R, Middelkoop E. Collagen morphology in human skin and scar tissue: no adaptations in response to mechanical loading at joints. Burns. 2003;29(5):423–31.

Vawter DL, Fung YC, West JB. Elasticity of excised dog lung parenchyma. J Appl Physiol. 1978;45(2):261–9.

Viidik A. Biology of Collagen. Viidik A, Vuust J, editors. London: Academic Press; 1980;239–355

Wilkes GL, Brown IA, Wildnauer RH. The biomechanical properties of skin. CRC Crit Rev Bioeng. 1973;1(4):453–95.

Wright DG, Rennels DC. A study of the elastic properties of planar fascia. J Bone Joint Surg. 1964;46:482–92.

Yin FC, Strumpf RK, Chew PH, Zeger SL. Quantification of the mechanical properties of non-contracting canine myocardium under simultaneous biaxial loading. J Biomech. 1987;20(6): 577–89.

Young AA, LeGrice IJ, Young MA, Smaill BH. Extended confocal microscopy of myocardial laminae and collagen network. J Microsc. 1998;192:139–50.